Cellular Physiology and Biochemistry

Cell Physiol Biochem 2018;47:1509-1532
DOI: 10.1159/000490867
Published online: June 25, 2018
Accepted: April 24, 2018

Original Paper

$G\alpha_i$ Proteins are Indispensable for Hearing

Sandra Beer-Hammer[a] Sze Chim Lee[b] Stephanie A. Mauriac[c,d] Veronika Leiss[a] Isabel A. M. Groh[a] Ana Novakovic[a] Roland P. Piekorz[e] Kirsten Bucher[a] Chengfang Chen[b] Kun Ni[b] Wibke Singer[b] Csaba Harasztosi[f] Thomas Schimmang[g] Ulrike Zimmermann[b] Klaus Pfeffer[h] Lutz Birnbaumer[i,j] Andrew Forge[k] Mireille Montcouquiol[c,d] Marlies Knipper[b] Bernd Nürnberg[a] Lukas Rüttiger[b]

[a]Department of Pharmacology and Experimental Therapy, and Interfaculty Center of Pharmacogenomics and Drug Research (ICePhA), University of Tübingen, Tübingen, Germany, [b]Molecular Physiology of Hearing, Tübingen Hearing Research Centre, Department of Otolaryngology, University of Tübingen, Tübingen, Germany; [c]INSERM, Neurocentre Magendie, U1215, 146 rue Leo-Saignat, Bordeaux, [d]University of Bordeaux, Neurocentre Magendie, Bordeaux, France; [e]Institute for Biochemistry and Molecular Biology II, Medical Faculty, University of Düsseldorf, Düsseldorf, Germany, [f]Department of Otolaryngology, Tübingen Hearing Research Center, Section of Physiological Acoustics and Communication, University of Tübingen, Tübingen, Germany; [g]Instituto de Biologíay Genética Molecular, Universidad de Valladolid y Consejo Superior de Investigaciones Científicas, Valladolid, Spain; [h]Institute of Medical Microbiology and Hospital Hygiene, University of Düsseldorf, Düsseldorf, Germany; [i]Neurobiology Laboratory, National Institute of Environmental Health Sciences, National Institute of Health, Research Triangle Park, USA; [j]Institute of Biomedical Research (BIOMED), School of Medical Sciences, Catholic University of Argentina, Buenos Aires, Argentina; [k]UCL Ear Institute, London, UK

Key Words
Heterotrimeric G-proteins • $G\alpha_{i3}$/GNAI3 • Stereocilia bundle • Cochlear hair cell maturation • Neural gain • Deafness gene

Abstract
Background/Aims: From invertebrates to mammals, $G\alpha_i$ proteins act together with their common binding partner Gpsm2 to govern cell polarization and planar organization in virtually any polarized cell. Recently, we demonstrated that $G\alpha_{i3}$-deficiency in pre-hearing murine cochleae pointed to a role of $G\alpha_{i3}$ for asymmetric migration of the kinocilium as well as the orientation and shape of the stereociliary ("hair") bundle, a requirement for the progression of mature hearing. We found that the lack of $G\alpha_{i3}$ impairs stereociliary elongation and hair bundle shape in high-frequency cochlear regions, linked to elevated hearing thresholds for high-frequency sound. How these morphological defects translate into hearing phenotypes is not clear. ***Methods:*** Here, we studied global and conditional *Gnai3* and *Gnai2* mouse mutants deficient for either one or both $G\alpha_i$ proteins. Comparative analyses of global versus Foxg1-driven conditional mutants that mainly delete in the inner ear and telencephalon in combination with functional tests were applied to dissect essential and redundant functions of different $G\alpha_i$ isoforms and to assign specific defects to outer or inner hair cells, the auditory nerve, satellite

Prof. Dr. Dr. Bernd Nürnberg
and PD Dr. Lukas Rüttiger

Department of Pharmacology and Experimental Therapy, University Tübingen,
Wilhelmstr. 56, D-72074 Tübingen (Germany); Tel. +49 7071 2974590,
E-Mail bernd.nuernberg@uni-tuebingen.de / lukas.ruettiger@uni-tuebingen.de

cells or central auditory neurons. ***Results:*** Here we report that lack of $G\alpha_{i3}$ but not of the ubiquitously expressed $G\alpha_{i2}$ elevates hearing threshold, accompanied by impaired hair bundle elongation and shape in high-frequency cochlear regions. During the crucial reprogramming of the immature inner hair cell (IHC) synapse into a functional sensory synapse of the mature IHC deficiency for $G\alpha_{i2}$ or $G\alpha_{i3}$ had no impact. In contrast, double-deficiency for $G\alpha_{i2}$ and $G\alpha_{i3}$ isoforms results in abnormalities along the entire tonotopic axis including profound deafness associated with stereocilia defects. In these mice, postnatal IHC synapse maturation is also impaired. In addition, the analysis of conditional versus global $G\alpha_{i3}$-deficient mice revealed that the amplitude of ABR wave IV was disproportionally elevated in comparison to ABR wave I indicating that $G\alpha_{i3}$ is selectively involved in generation of neural gain during auditory processing. ***Conclusion:*** We propose a so far unrecognized complexity of isoform-specific and overlapping $G\alpha_i$ protein functions particular during final differentiation processes.

Introduction

Heterotrimeric G-proteins are grouped into four subfamilies, i.e. $G\alpha_i$, $G\alpha_s$, $G\alpha_q$, and $G\alpha_{12/13}$, according to the nature of their α subunit, which also reflects their specificity for distinct G-protein-coupled receptors and sets of effector proteins [1, 2]. The three mammalian $G\alpha_i$ isoforms, i.e. $G\alpha_{i1}$, $G\alpha_{i2}$, $G\alpha_{i3}$, are best described as being the inhibitory Gα subunits that suppress adenylyl cyclase activity resulting in decreased cellular cAMP levels [3-5]. In addition, specific binding partners such as members of the activators of G-protein signaling (AGS) family have emerged as crucial intracellular regulators that can control G-protein activity even in the absence of GPCR-stimulation. Until now, $G\alpha_i$ isoforms together with Gpsm2 (also known as AGS5, LGN), a group II AGS/guanine nucleotide dissociation inhibitor (GDI) [6, 7], have been implicated in signaling pathways that control mitotic spindle dynamics and thereby asymmetric cell division, polarity, growth and differentiation in invertebrates up to mammalian cells [8-12]. Initially, Gpsm2 was found in functional screens as a receptor-independent activator of G-protein-signaling interacting with GDP-bound $G\alpha_{i2}$ through its four $G\alpha_{i/o}$-loco motifs [13, 14]. Subsequently, this interaction was demonstrated for all three $G\alpha_i$ isoforms at least *in vitro* [15]. Inhibiting Gα protein function with the pan-$G\alpha_{i/o}$-blocker PTX or *via* expression of an Atoh1-PTX construct demonstrated that $G\alpha_i$ and Gpsm2 control kinocilium migration and planar organization of stereociliary bundles in the hair cells of the murine cochlea [16, 17]. Gpsm2 dysfunction has been linked to mutations in the *GPSM2* gene in patients, formerly known as the deafness locus DFNB82, responsible for the autosomal recessive disorder Chudley-McCullough-syndrome [18, 19] that is characterized by severe to profound congenital hearing loss in humans [20-22]. Moreover, knock-out mice revealed that the deletion of the $G\alpha_{i3}$ isoform was sufficient to mimic the PTX phenotype in the immature pre-hearing organ by disrupting the migration of the kinocilium at the surface of hair cells and affecting hair bundle orientation and shape [16]. So far, $G\alpha_{i3}$ *per se* has not been associated with hereditary deafness because of an assumed functional $G\alpha_i$ isoform redundancy for hearing. Nevertheless, we and others recently reported hearing loss in $G\alpha_{i3}$ cKO and Atoh1-PTX mice, correlating with stereociliary elongation defects in IHCs [19, 23]. It remains open whether the ubiquitously expressed Gpsm2-binding partner $G\alpha_{i2}$ has also an impact on cochlear architecture and auditory function and whether both $G\alpha_i$ proteins play specific and/or redundant roles.

Here, we examined the physiological role of $G\alpha_i$ isoforms for hearing by using gene-targeted mouse lines for $G\alpha_{i2}$, $G\alpha_{i3}$ and $G\alpha_{i2}/G\alpha_{i3}$ and transgenic reporter mice expressing $G\alpha_{i3}$-GFP. Comparative analyses of global versus conditional mutants that mainly delete in the inner ear and the telencephalon in combination with functional tests allowed us to dissect essential and redundant functions of different $G\alpha_i$ isoforms and to assign specific defects to outer or inner hair cells, the auditory nerve, satellite cells or central auditory neurons. We show that both $G\alpha_{i2}$ and $G\alpha_{i3}$ act in a spatially and functionally complex manner not only on planar organization of hair cell bundles, but are also required for final differentiation

of the first auditory synapse (the inner hair cell), and central neural gain during auditory processing. Therefore, hearing loss associated with dysfunction of specific $G\alpha_i$ isoforms is not only caused by abnormal stereociliary bundle or mitotic spindle organization but may also be a consequence of the disability for postnatal neuronal maturation and central adaptation.

Materials and Methods

Animals

Adult (1- to 8-month-old) mice weighing 15-35 g were included in this study. For all mouse lines, male and female animals were used, because we did not observe sex-dependent differences. The use, treatment and care of the animals and the experimental protocols were based on the institutional guidelines of the Veterinary Care Unit, University of Tübingen and were approved by the animal welfare commissioner of the regional board for scientific animal experiments in Tübingen (PH7/14). Experiments were performed according to the European Union Directive 86/609/EEC for the protection of animals used for experimental and other scientific purposes. Mice were kept according to national guidelines for animal care in an specific-pathogen free (SPF) animal facility.

Gene targeting and mice

For generation of *Gnai3*$^{fl/fl}$ mice, E14.1 embryonic stem (ES) cells from 129/Ola mice were grown in Dulbecco's modified Eagle's medium (Invitrogen, Carlsbad, CA, USA) supplemented with 2 mM glutamine (Seromed, Wien, Austria), leukemia inhibitory factor, 100 U/ml penicillin, 100 µg/ml streptomycin (Seromed), 50 µM 2-mercaptoethanol (Invitrogen) and 15% heat-inactivated fetal bovine serum (Pan Biotech, Aidenbach, Germany). Genomic fragments flanking the murine *Gnai3* gene as well as *TK-neomycin* and *diphtheria toxin A* (*DTA*) were cloned into pBluescript (Agilent technologies, Santa Clara, CA, USA) and fully sequenced. The targeting vector was designed according to the *Gnai3* knockout construct, where exon 6 is deleted [24]. Therefore, exon 6 of the *Gnai3* gene was flanked by loxP-sequences. At the 3' site, the loxP-flanked *TK-Neo* resistance cassette was inserted in reverse orientation in intron 6 of the *Gnai3* gene without deleting any endogenous sequence. Additionally, after the short arm, which encodes exon 7, a DTA cassette was inserted for the negative selection of ES cell clones (for all online suppl. material, see www.karger.com/doi/10.1159/000490867, suppl. Fig. 1). E14.1 ES cells were electroporated with the NotI-linearized targeting vector, and the transfected cells were subsequently subjected to G418 and Ganciclovir selection. Clones carrying the correct homologous recombination were identified by Southern blot hybridization with the 5' flanking probe (5´fp) indicated in (see online suppl. material) suppl. Fig. 1 after digestion of ES cell DNA with PstI (data not shown). Single integration was verified by digestion with BamHI and probing the Southern blot with the *neomycin* resistance cassette. Thereafter, the selected positive clones were transfected with Cre-recombinase to delete the loxP-flanked *TK-Neo* resistance cassette. Clones were selected by Ganciclovir treatment allowing for clones growing only when the *TK-Neo* resistance cassette was successfully excised. The selected clones were again checked with Southern blot hybridization with the internal probe P2 (3´fp2, see online suppl. material, suppl. Fig. 1A) after digestion with PstI (data not shown). Correctly targeted ES cell clones were injected into C57BL/6 blastocysts, which were transferred into pseudopregnant foster mice. Resulting chimeric mice were backcrossed to C57BL/6 mice, and germ line transmission of the targeted allele was again confirmed by Southern blot analysis. *Gnai3*$^{fl/fl}$ mice were backcrossed to the C57BL/6 genetic background for at least five generations. Genotyping of *Gnai3*$^{fl/fl}$ mice was performed by PCR with the following primers: 5'-GCAATTATCTTTTGTGTGGC-3' (Ex6-F); 5'-ATGCTGTCAAACAATTTCATGC-3' (Ex7-R); 5'-TAGCAGTTGTCATGGCTACC-3' (Int-F) (see also online suppl. material, suppl. Table 1). The recombined allele results in a band of 350 bp (see online suppl. material, suppl. Fig. 1 B and C). To check successful deletion of *Gnai3*, mice were crossed with *Ella-Cre* mice and PCR analysis confirmed deletion of *Gnai3* (see online suppl. material, suppl. Fig. 1B and C). A specific deletion of *Gnai3* or *Gnai2* in the inner ear and telencephalon was achieved by crossing *Gnai3*$^{fl/fl}$ or *Gnai2*$^{fl/fl}$ mice and *Foxg1-Cre* mice. *Gnai2*$^{fl/fl}$ mice were provided by the Comparative Medicine Branch of the National Institute of Environmental Health Sciences, North Carolina 27709 [25], backcrossed on a C57BL/6N background [26], and the *FoxG1-Cre* mouse line [27] was purchased from The Jackson Laboratory (Bar Harbor, ME, USA), on a C57BL/6N background. A tissue-specific mutant mouse line was generated where both *Gnai*

genes were disrupted by crossing with the *FoxG1-Cre* mouse line. *Gnai2*$^{fl/fl}$; *Gnai3*$^{fl/fl}$; Foxg1-Cre^{neg} littermates were used as controls. Genotyping of Gnai2$^{fl/fl}$ mice was performed by PCR with the following primers: for: 5'-GGCTATGATCCCAAAACTCCCCG-3' and rev: 5'-GTGGTAAGCCTGTGTTTGTGAGAG-3'. The recombined allele results in a band of 420 bp (data not shown).

Gnai3-GFP mutant mice were generated in collaboration with Cyagen Biosciences and a more detailed description will be described elsewhere (Beer-Hammer *et al*, in preparation). Briefly, the eGFP-cDNA was inserted in Exon 8 of *Gnai3* right after the TGA stop codon. To achieve equal expression of $G\alpha_{i3}$ and eGFP the construct contains an IRES (internal ribosomal entry site). With this we achieve an equivalent expression of $G\alpha_{i3}$ and GFP. The GFP expression was successfully detectable via flow cytometry (data not shown) and immunohistochemistry (this study). *Gnai3*-GFP mutant mice are born and grow without any obvious signs of abnormalities.

Organismal ("global") *Gnai*-deficient mice were originally provided by the Comparative Medicine Branch of the National Institute of Environmental Health Sciences, North Carolina 27709 on a genetic SV129 background [28]. Subsequently, the mouse strains were backcrossed on a C57BL/6N background for at least nine generations [26, 29]. The *Gnai2* mutant mouse line was kept in Individually Ventilated Cages (IVC), while the *Gnai3* mutant mouse line was kept under SPF conditions. Generation and initial characterization of global and conditional *Gnai2*- or global *Gnai3*-deficient mice is described in detail in [16, 24, 30].

Hearing tests

Hearing was tested on anesthetized animals through auditory brainstem response (ABR) measurements of the distortion product otoacoustic emissions (DPOAE), and electrocochleography. ABR to click and pure tone stimuli and the cubic 2*f1–f2 DPOAE for f2=1.24*f1 and L2=L1–10 dB were recorded in adult 1- to 8-month-old anesthetized mice. From click-evoked ABRs, consecutive wave components that reflect the summed neural activity along the ascending auditory pathway were analyzed as described [31-33]. *In vivo* electrocochleography (compound action potentials of the auditory nerve, CAP; summating potential of IHC receptor potentials, SP; receptor potential of OHCs, cochlear microphonic, CM) was performed in anesthetized mice as described [34]. From the waveform signal of the CAP and CM recordings, peak amplitudes (in mV) were calculated and plotted as input/output (I/O) functions with increasing stimulus level (0–100 dB SPL). For CM I/O function, peak-to-peak amplitudes were calculated for the stimulus frequency of 16 kHz, the stimulus frequency giving the best response. For SP, amplitude was defined as average DC potential minus baseline for stimulus frequency at 11.3 kHz.

SEM and measurements

The inner ear (cochlear and vestibular system) of mice aged P21 were harvested and immersed in 2.5% glutaraldehyde in 0.1M cacodylate buffer, pH 7.35, with 3mM CaCl2 for 24 h or more. The tissues were postfixed in 1% OsO4 in the same buffer, dissected and double processed with thiocarbohydrazide followed by OsO4 [35] before dehydration through an alcohol series and critical point drying with CO_2. After mounting on specimen support stubs, samples were sputter coated with platinum. Samples were examined with a JEOL 6700 F cold field emission scanning electron microscope operating at 3 or 5 kV. Measurements were made on the longest row of stereocilia closest to the kinocilium.

Stereocilia length was estimated in 20 (control) and 11 (*Gnai3* cKO) independent experiments in tissue samples from 4 control and 4 *Gnai3* cKO mice, respectively. Only if the length of at least 4 stereocilia could be determined, the value was considered for the statistical analysis. Stereocilia length could be derived from a total of 64 hair cells of control mice and 64 hair cells of *Gnai3* cKO mice. A total of 272 stereocilia and 305 stereocilia could be measured for control and *Gnai3* cKO mice, respectively. Stereocilia number per hair cell was counted in 12 and 14 independent experiments (countings) for 5 control and 4 *Gnai3* cKO mice, respectively. Each stereocilia counting included at least 4 hair cells. From a total of 87 and 106 hair cells from control and *Gnai3* cKO mice, a total of 8299 and 7621 stereocilia could be counted, respectively

Images were collected from the basal or middle turn of the cochlea, defined as B20/30% and 50/60% of the total length of the organ of Corti from the base. At each location, the hair bundles were viewed both from behind the longest row of stereocilia to view the height of the hair bundle as well as approximately perpendicular to the apical surface of the HC or toward the inner aspect of the bundle to examine its overall morphology and composition. To estimate bundle height, measurements were made from images at calibrated instrument magnifications of 20, 000 or occasionally 10, 000. Although we might have underestimated the

actual stereocilia length, all efforts were taken to minimize the effect of parallax. Measurements were taken from bundles viewed from the lateral side toward the medial side (from the stria toward the modiolus), so that the row of longest stereocilia were imaged from the 'rear.' Samples were tilted and rotated so that the row of longest stereocilia was approximately perpendicular to the direction of view. Stereo-imaging was used in a few cases to gain an indication of possible errors in length measurements from 2D images. From the anaglyphs generated by a pair of images separated by 8 degrees of tilt, height measurements were obtained using analySIS software. These revealed little difference in the height measurement from that obtained from the 2D image of a stereocilium at close to perpendicular to its long axis. Measurements were made using ImageJ software.

Tissue preparation and Immunohistochemistry

Murine and rat cochlear tissues were prepared as whole-mounts or cryosections for the purpose of immunohistochemistry. Cochleae were isolated, fixed by immersion in 2% paraformaldehyde, 125 mM sucrose in 100 mM phosphate buffered saline, pH 7.4, for 2 h and then decalcified for 45 min in RDO rapid decalcifier (Apex Engineering Products Corporation, Aurora, IL, USA) as described [31, 36, 37], cryosectioned at 10 µm and mounted on SuperFrost*/plus microscope slides (R. Langenbrinck Labor- u. Medizintechnik, Emmendingen, Germany) at –20°C. For whole-mount preparation, we dissected cochlear turns and mounted them on slides with the tissue adhesive Cell-Tek (BD Bioscience, Schwerte, Germany) in PBS and performed phalloidin labeling as described [38]. For immunohistochemistry and LacZ staining, mouse cochlear sections were stained as previously described [31, 37, 39]. BK (KCa1.1) (rb, Alomone Labs, Jerusalem, Israel), CtBP2/RIBEYE (rb, American Research Products, Waltham, MA, USA), KCNQ4 (rb, [40, 41], Nf200 (ms), SK2 (rb), Kir.4.1 (ms) all three from Sigma, otoferlin (ms, LifeSpan BioSciences, Seattle, WA, USA), prestin (gt, Santa Cruz Biotechnology, Dallas, TX, USA), Sox10 (gt, Santa Cruz biotechnology, Dallas, TX, USA), VAMP2 and brevican (ms) from BD Bioscience and vGLUT1 (rb) both from Synaptic Systems (Göttingen, Germany), espin (ms, Fisher Scientific, Schwerte, Germany), $G\alpha_{i1/i2}$ and $G\alpha_{i3}$-specific antibodies [29], and GFP (rb, Novus Biologicals, Littleton, CO, USA) were used as primary antibodies for localizing the respective proteins in the inner ear, see also online suppl. material, suppl. Table 1. All commercial antibodies were used as recommended by the manufacturers. $G\alpha_{i1/i2}$ and $G\alpha_{i3}$-specific antibodies have been routinely validated with immunoblot and immunohistochemistry on wildtype and appropriate $G\alpha_i$-deficient tissues [19, 29, 42]. For double labeling studies, both antibodies were simultaneously incubated for identical time periods. Hair cell stereocilia bundles were visualized by fluorescent phalloidin labeling of F-actin (Alexa Fluor 568 Phalloidin, Molecular Probes, Eugene, OR, USA). Sections and whole-mounts were viewed as described [43] using an Olympus BX61 microscope (Olympus, Hamburg, Germany) equipped with epifluorescence illumination. Images were acquired using an Olympus XM10 CCD monochrome camera and analyzed with cellSens Dimension software (OSIS GmbH, Münster, Germany). To increase spatial resolution, slices were imaged over a distance of 15 µm within an image-stack along the *z*-axis (*z*-stack) followed by 3-dimensional deconvolution using cellSens Dimension built in algorithm.

Tissue preparation and Immunoblot

Liquid-frozen cerebellum and brain stem were homogenized in 500 µl protein lysis buffer (20 mmol/l Tris, pH 8.3; 0.67% SDS; 238 mmol/l 2-mercaptoethanol; 0.2 mmol/l PMSF). To achieve electrophoretical separation of $G\alpha_i$ isoforms, separation was performed in gels containing 6 M urea. The proteins were visualized by immunodetection using the following primary antibodies described elsewhere [29] rabbit anti-$G\alpha_{i1/i2}$ (7.2 ng/ml), rabbit anti-$G\alpha_{i3}$ (50 ng/ml). Finally, to visualize equal loading membranes were stained with Amido black.

Experimental Design and Statistical analysis

Data are presented as mean with standard deviation (SD) or mean with standard error of the mean (SEM). In the Figures, error bars are presented with and without caps for SD and SEM, respectively. Details for all statistical analyses are provided (see online suppl. material) in suppl. Table 2. In brief: differences of the mean were compared for statistical significance pair-wise by student's *t*-test (click-ABR thresholds in Fig. 1F and see online suppl. material, suppl. Fig. 2; ABR slope in Fig. 7B-C and see online suppl. material, suppl. Fig. 3B and C; loss of ABR threshold over age in Fig. 7D) or multiple comparisons 2-way ANOVA for factor "genotype" followed by post-hoc comparisons with Bonferroni's multiple comparison test (f-ABR in

Fig. 1A-E; DPOAE thresholds and amplitudes in Fig. 2; electrocochleography in Fig. 5; ribbon counting in Fig. 6D; ABR amplitude I/O and latency I/O in Fig. 7B and C and (see online suppl. material) suppl. Fig. 3B and C; ABR wave IV/I ratios in Fig. 7E and (see online suppl. material) suppl. Fig. 3D. Fisher's exact test for associations was performed for 2x2 contingency tables (Fig. 1F, and stereocilia orientation in Fig. 3B). Non-parametric Mann-Whitney test was used to compare for statistical significance of stereocilia number and length in Fig. 3E and (see online suppl. material) suppl. Table 3. Unless otherwise noted, statistical significance was tested at the level of 5%. Level of significance is illustrated in the Figures with symbols or shaded areas (n.s. $p > 0.05$; *$p < 0.05$; **$p < 0.01$; ***$p < 0.001$) and depicted in (see online suppl. material) suppl. Table 2. For Student´s t-test, 2-way ANOVA Graph by Mann-Whitney test, and Kruskal-Wallis test Pad Prism 6.01 (GraphPad Software, Inc. La Jolla, CA, USA) was used. For the Fisher´s exact test the online tool of vassarstats (http://vassarstats.net/tab2x2.html) was used.

Results

Isoform–specific and redundant roles of $G\alpha_i$ proteins for high- and low-frequency hearing and hair bundle organization

The functional consequences of deficiency for different $G\alpha_i$ isoforms for auditory responses was explored by special hearing tests. The auditory brainstem response (ABR) was measured in response to click and pure tone auditory stimuli in 1- to 3-month-old mice with global (g) or conditional (c) absence of $G\alpha_{i2}$ and/or $G\alpha_{i3}$. Conditional mouse mutants lacking one or both isoforms were generated by Cre-driven recombination using the Foxg1 promoter [27]. *Gnai2* gKO (Fig. 1A) and *Gnai2* cKO (Fig. 1B) mice both displayed tone-burst evoked ABR thresholds (f-ABR) and click-evoked ABR thresholds (Fig. 1F, click-ABR) similar to controls, suggesting that $G\alpha_{i2}$ is either dispensable for hearing or may be functionally substituted by remaining $G\alpha_i$ isoforms. In contrast, *Gnai3* gKO (Fig. 1C) and *Gnai3* cKO (Fig. 1D) mice demonstrated a significant elevation of f-ABR and click-ABR thresholds towards higher frequency regions. This suggests a selective role of $G\alpha_{i3}$ particularly for these frequencies, which cannot be rescued by $G\alpha_{i2}$. In order to identify

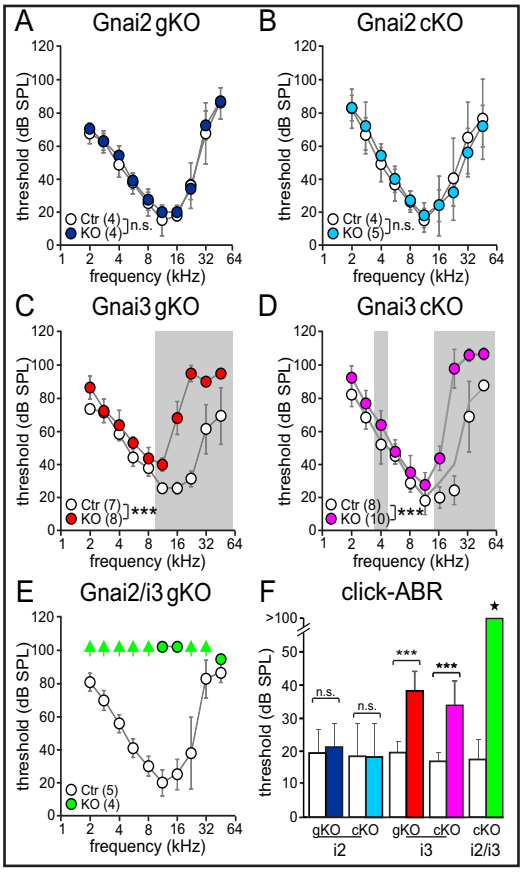

Fig. 1. ABR thresholds of gene-targeted *Gnai* KO mice. (A-E) Frequency tone-burst-evoked ABR (f-ABR) thresholds, mean±SD from 4 to 8 mice (number of ears in brackets). (A,B) Frequency tone-burst-evoked ABR thresholds were not affected in (A) global (gKO) and (B) tissue-specific (cKO) *Gnai*2 KO mice. (C,D) High-frequency loss occurs in (C) *Gnai3* gKO and (D) cKO. ABR thresholds in *Gnai*3 gKO and cKO are significantly elevated for stimulation frequencies above 8 kHz (shaded areas, $p < 0.05$). (E) Profound ABR threshold loss was found in *Gnai*2/i3 cKO mice over all stimulus frequencies. Arrows indicate ABR thresholds exceeding the maximum tested stimulus level. (F) Click-evoked ABR (click-ABR) thresholds for the mice mutants (global deletion of *Gnai*2, dark blue, conditional deletion of *Gnai2*, light blue, global deletion of *Gnai*3, red, conditional deletion of *Gnai*3, purple, conditional double deletion of *Gnai2*/i3, green) vs. their respective controls (white). n.s. not significant, "star" $p < 0.05$, "***" $p < 0.001$. Detailed statistic is depicted in (see online suppl. material) suppl. Fig. 2 and suppl. Table 2.

overlapping functions between $G\alpha_{i2}$ and $G\alpha_{i3}$ we next analyzed mice defective for both genes. As mice with a global deficiency for both *Gnai2* and *Gnai3* are embryonic lethal [29] we generated conditional *Gnai2/i3* cKO mice that were viable and allowed inspection of hearing functions in the adult animal. Rather unexpectedly, *Gnai2/i3* cKO mice were profoundly deaf (Fig. 1E) with click-ABR thresholds that consistently exceeded 100 dB sound pressure level (SPL, root mean square weighted for click stimuli, SPL_{rms}) (Fig. 1F and see online suppl. material, suppl. Fig. 2). Indeed, in comparison to *Gnai2/i3* cKO mice the hearing thresholds of global and conditional *Gnai3* mutants were only significantly elevated while that of global or conditional *Gnai2* mutants were normal (Fig. 1F and see online suppl. material, suppl. Fig. 2).

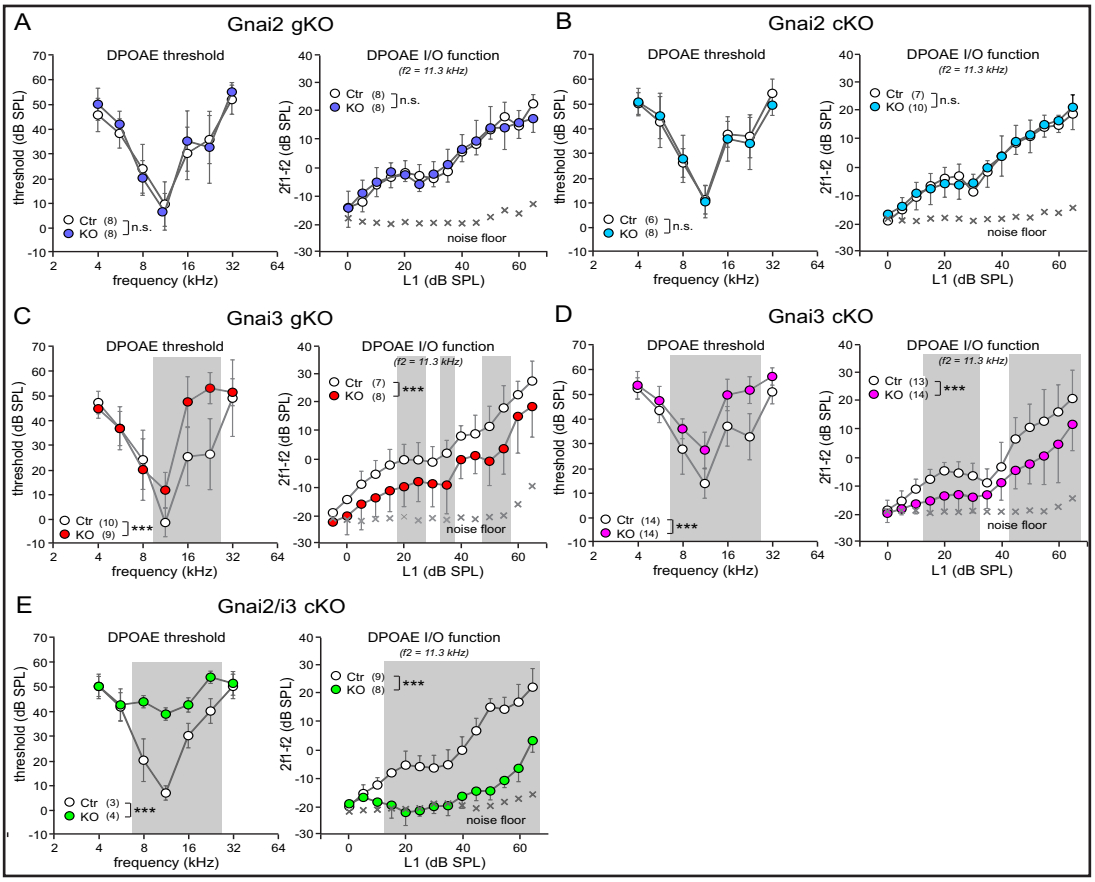

Fig. 2. DPOAE thresholds and DPOAEs amplitude I/O function in *Gnai*2 and *Gnai*3 gene-targeted mice. (A,B) OHC function in global and tissue-specific *Gnai*2 KO is not impaired. Mean±SD DPOAE thresholds (left panels) and DPOAEs amplitude I/O function evoked by stimulus f2=11.3 kHz (right panels) above noise floor (crosses) for *Gnai*2 gKO (A, KO) and *Gnai*2 cKO mice (B, KO) and their respective controls (Ctr) are similar. (C,D) Impairment of OHC function at high-frequency regions in global and tissue-specific *Gnai*3 KO mice. Mean±SD DPOAE thresholds (left panels) and DPOAEs amplitude I/O function (right panels) for *Gnai*3 gKO (C) and *Gnai*3 cKO mice (D), and their respective controls. DPOAE thresholds for stimulation frequencies above 8 kHz are significantly elevated and DPOAE amplitudes were significantly reduced in KO mice compared to the respective controls. (E) OHC function is lost in *Gnai*2/i3 cKO mice. Mean±SD DPOAE thresholds (left panels) and DPOAEs amplitude I/O function evoked by stimulus f2=11.3 kHz (right panels) for *Gnai*2/i3 cKO and their respective controls. Remarkable loss of thresholds at most testing frequencies and reduction of amplitudes are evident. Grey-shaded areas represent statistically significant post-hoc comparisons with $p< 0.05$ after Bonferroni corrections. "n.s." and "***" indicate level of statistical significance $p> 0.05$ and $p< 0.001$, respectively. Data points represent the mean of 6 to 14 ears (numbers in brackets close to legend key) from 4 to 7 mice (A-D) and 3 to 4 ears from 2 mice (E).

To validate the specific contribution of outer hair cells (OHCs) to this hearing threshold difference in *Gnai* mutant mice, distortion product otoacoustic emissions (DPOAE) thresholds were measured as a metric of intact OHC mechanoelectrical response [44]. As expected from normal ABR thresholds seen in *Gnai2* gKO and *Gnai2* cKO mouse models (Fig. 1A and B) normal input/output (I/O) functions of emission amplitudes evoked by stimulus frequency f2=11.3 kHz were also observed in both *Gnai2* KO lines (Fig. 2A and B). Global (Fig. 2C) and conditional (Fig. 2D) *Gnai3* KO mice had significantly elevated DPOAE thresholds at test frequencies from 8 to 22.6 kHz (Fig. 2C and D, left panel) and exhibited reduced emission amplitudes at f2=11.3 kHz (Fig. 2C and D, right panel). Both observations indicate that the elevated hearing thresholds in these *Gnai* mouse mutants (Fig. 1C and D) are related to impaired mechanoelectrical OHC properties in high-frequency cochlear regions.

In contrast to single *Gnai2* KO and *Gnai3* KO, *Gnai2/i3* cKO mice displayed residual DPOAEs only for the highest stimulus intensities at f2=11.3 kHz with significantly reduced emission amplitudes (Fig. 2E). This indicates that both $G\alpha_{i2}$ and $G\alpha_{i3}$ are essential for hearing and that $G\alpha_{i2}$ can functionally replace $G\alpha_{i3}$ in low frequency but not in high frequency regions.

Furthermore, to specify the role of $G\alpha_i$ for hair bundle organization we next examined the shape of OHC hair bundles in young *Gnai3* gKO mice around hearing onset (P11-12) by using phalloidin staining to visualize actin in stereocilia (Fig. 3A) and categorized their shape in terms of the angle between the hair bundle arms (Fig. 3B). A significantly higher number of OHCs with wider V-shaped stereociliary bundles exceeding 110° was found in basal (high-frequency) cochlear turns of *Gnai3* gKO compared to control mice whereas the visible differences were statistically insignificant in apical (low-frequency) cochlear turns. The quantification is shown in lower panel of Fig. 3B. Scanning electron microscopy, performed in cochlear samples obtained at P21 from *Gnai3* cKO confirmed abnormal bundles in basal but no obvious anomaly in apical (low-frequency) cochlear turns were found (Fig. 3C and D). Additionally, there were shorter and fewer stereocilia on OHCs in basal cochlear turns of *Gnai3* cKOs (Fig. 3E and see online suppl. material, suppl.Table 3). *Gnai2/i3* double-deficiency induced hair bundle shape abnormalities also in the apical cochlear turn (Fig. 3F) as shown by fluorescence microscopy using phalloidin and espin as stereocilia markers.

Next, we examined if the hair bundle abnormalities are linked to expression profiles of the different $G\alpha_i$ isoforms. These abnormalities were restricted to higher frequency regions in *Gnai3* cKO mice whereas they extended over high and low frequency regions in *Gnai2/i3* cKO mice. The expression profiles of $G\alpha_{i2}$ (Fig. 4A and B) and $G\alpha_{i3}$ (Fig. 4C and D) were analyzed by immunohistochemistry in whole-mount preparations of the rat cochlea. At P2, $G\alpha_{i3}$ was detected in inner hair cell (IHC) and OHC hair bundles throughout the cochlear length, while $G\alpha_{i2}$ immunoreactivity was restricted to the apical turn (Fig. 4A and C). At P10, both $G\alpha_{i2}$ and $G\alpha_{i3}$ expression was evident in the apical turn, while $G\alpha_{i3}$ dominated mainly in the basal turn (Fig. 4B and D). The strong expression of $G\alpha_{i3}$ in hair bundles in basal high-frequency cochlear turns and the co-expression of $G\alpha_{i2}$ and $G\alpha_{i3}$ in hair bundles in apical lower-frequency cochlear turns thus support the idea that $G\alpha_{i2}$ does not substitute for *Gnai3*-deficiency in basal cochlear turn, which may explain the distinct hearing deficits in *Gnai* mouse mutants.

Abnormal hair bundle elongation in the *Gnai3*-deficient mice may lead to hearing deficits through dysfunctional mechanoelectrical transduction (MET). The functionality of MET and the electrical potential from the subsequent initiated synchronous activation of the auditory nerve fibers can be captured by the steepness with which sound-induced compound action potentials of the auditory nerve (CAP) increase to escalating sound intensities and CAP threshold [45, 46]. To address if a disruption of stereociliary bundle elongation in *Gnai3* KO would impact the functionality of MET channels, we measured sound-induced CAP responses in age-matched *Gnai3* cKO and control mice. Best CAP thresholds of about 20 dB SPL at 11.3 kHz were found in control mice, and the growth functions for this stimulus frequency are shown in Fig. 5A. *Gnai3* cKO mice had significantly elevated CAP thresholds of >35 dB SPL and the CAP amplitude growth points to disturbed transduction of sound-induced mechanical signals (Fig. 5A). On average, the CAP amplitude reduction in *Gnai3* cKO mice was larger at

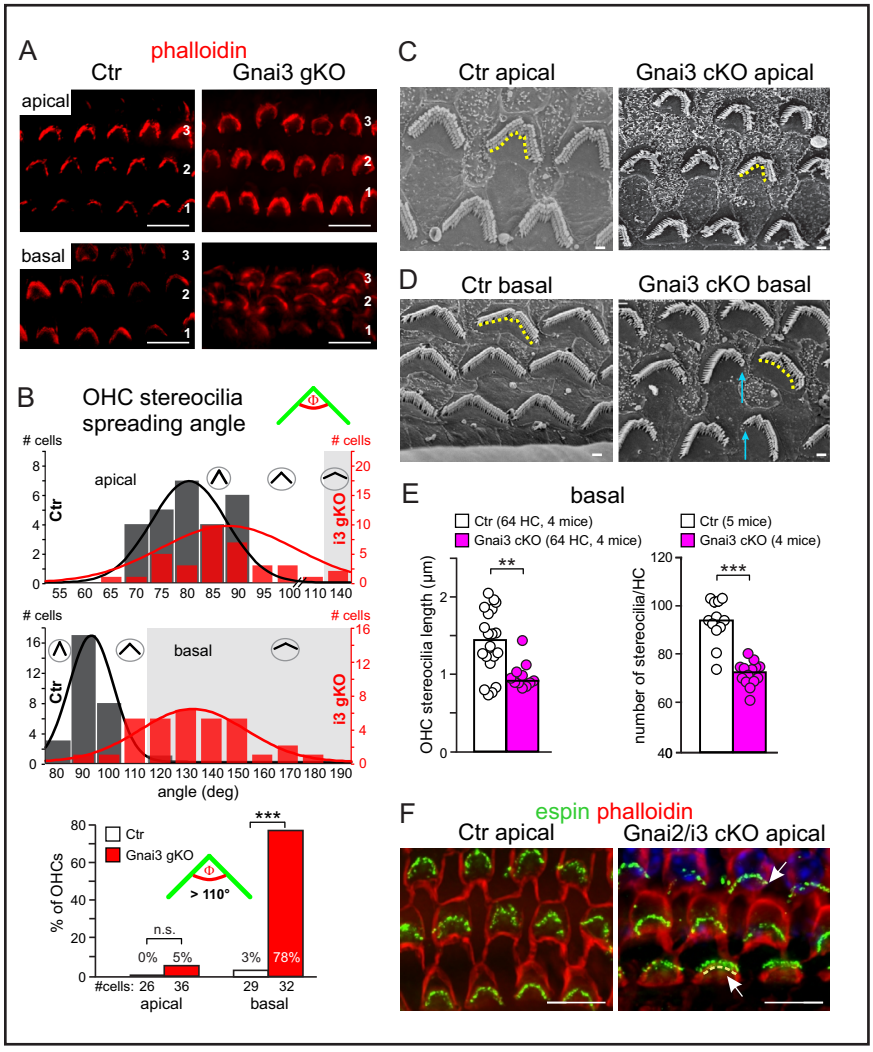

Fig. 3. Stereociliar configuration of OHCs in apical and basal cochlear turns from gene-targeted *Gnai* KO mice. (A) Phalloidin staining of control (Ctr, left panel) and *Gnai*3 gKO (right panel) OHC stereocilia bundles in P11-12 whole-mount cochlea for both cochlear turns. Scale bars 10µm. 3,2,1: OHC row. One representative animal of n=4-8 is shown. (B) Gaussian distribution of OHC stereocilia spreading angle for control (black) and *Gnai*3 gKO (red). *Gnai*3 gKO have significantly shallowed V-shaped bundles (Phi>110°) in basal turn OHCs, depicted by shaded area and encircled wide-spreaded chevron icons. Upper panel, OHCs from apical cochlear turn. Middle panel, OHCs from basal cochlear turn. Curves illustrate a fit of normal distribution for either group, ordinate gives absolute number of cells. Lower panel, quantification of OHCs with Phi>110° (%) of total cells analyzed (*Gnai*3 gKO 32-36 cells; *Gnai*3 ctr 26-29 cells). (C,D) Scanning electron microscopy of apical and basal stereocilia from control and *Gnai*3 cKO mice confirms normal hair bundle shape in apical cochlear turn (C) and the disorganized ultrastructure of OHC bundles from basal turns of *Gnai*3 cKO (D). Hair bundle shape is outlined in yellow. Blue arrows point to asymmetrically shaped bundles. Scale bars, 1µm. One representative animal of n=3 is shown. (E) Significantly reduced stereocilia length (left panel) and number (right panel) in basal cochlear turn of *Gnai*3 cKO mice. Stereocilia length was assessed in 20 (Ctr) and 11 (*Gnai3* KO) independent experiments (depicted as individual dots) in tissue samples from 4 control and 4 *Gnai3* KO mice. Stereocilia length was derived from a total of 64 hair cells of control mice and 64 hair cells of *Gnai3* KO mice. A total of 272 stereocilia and 305 stereocilia could be measured for control and KO mice, respectively. Stereocilia number per hair cell was counted in 12 and 14 independent experiments (countings depicted as dots) for 5 control and 4 *Gnai*3 KO mice, respectively. From 87 and 106 hair cells from control and *Gnai*3 KO mice, a total of 8299 and 7621 stereocilia could be counted, respectively. Stereocilia number ranged from 72-119 in control mice and 46-86 in *Gnai*3 KO mice. For both parameters median and single values are depicted. "**" and "***" indicate level of statistical significance p= 0.0107 and p< 0.0001, respectively. (F) Phalloidin (red) and espin (green) staining of *Gnai*2/i3 cKO OHC indicate abnormal bundle shape in apical low-frequency turns. Scale bars 10µm.

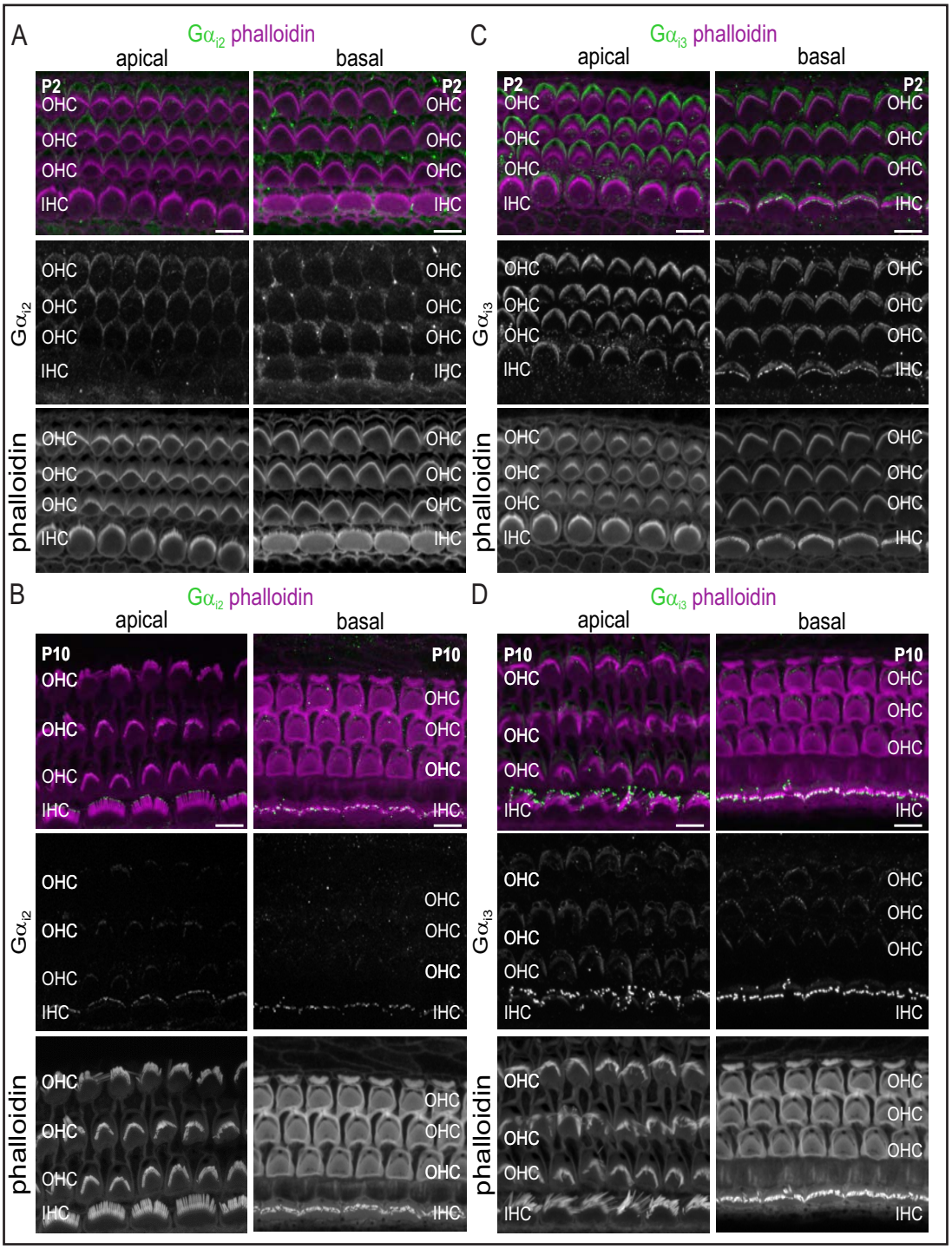

Fig. 4. Gα$_{i2}$ and Gα$_{i3}$ expression in the inner ear. (A-D) Surface view of whole-mount preparations of rat cochleae at P2 and P10. (A, B) Gα$_{i2}$ and (C,D) Gα$_{i3}$ labeling (green in upper panel and white in middle panel) in the actin-rich hair bundles labeled by phalloidin (purple in upper panel and white in lower panel). (A,C) At P2, Gα$_{i2}$ (A) and Gα$_{i3}$ (C) localizes at the tip of the OHC hair bundles in apical but only Gα$_{i3}$ in basal cochlear turns, whereas (B,D) at P10 Gα$_{i1/i2}$ (B) and Gα$_{i3}$ antibody (D) stains in IHCs in the apical but only Gα$_{i3}$ in the basal turn. Scale bars 7µm. One representative animal of n=5 is shown.

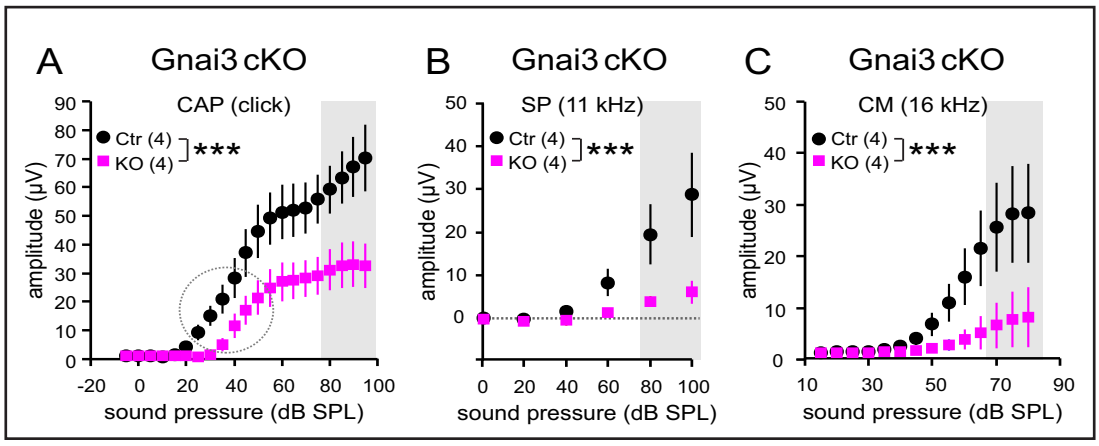

Fig. 5. Electrocochleography from gene-targeted *Gnai*3 KO mice. (A-C) Electrocochleographic responses of *Gnai*3 cKO mice are reduced by >2-fold confirming that the reduced cochlear output has its origin already at the receptor level (hair cell potentials). (A) Compound action potentials (CAP) - response from the auditory nerve. The circle highlights the similar slope of close-threshold CAP response growth. (B) summating potentials (SP) - determent potential from all hair cells. (C) cochlear microphonics (CM) - receptor potential of OHCs. Mean±SEM of 4 ears (4 mice). Differences of CAP, SP, and CM responses reach statistical significance at high stimulus levels (≥70dB SPL, shaded areas, $p<0.05$, post-hoc pair-wise Bonferroni's multiple comparison test). ***$p< 0.001$ for differences in factor genotype (2-way ANOVA for repeated measurements). Detailed statistic is depicted in (see online suppl. material) suppl. Table 2.

frequencies ≥ 16 kHz (~80%) than at lower frequencies ≤ 4 kHz (~50%) in comparison to age-matched controls (these growth functions are not shown as extra Figures). Moreover, the CAP responses were (right-)shifted to higher sound pressure levels in *Gnai3* cKO mice, albeit with similar steepness of amplitude growth (slope) from thresholds up to 50 dB SPL compared to control mice (Fig. 5A, CAP, encircled). Hence, mechanoelectrical currents in *Gnai3* cKO are likely to be functional in a limited response range but their sensitivity for activation seems to be impaired in high-frequency regions.

Failed activation of intact MET currents in high-frequency regions of *Gnai3* cKO mice was also confirmed by a barely detectable summation potential (SP) amplitude, that was recorded in *Gnai3* cKO mice at the round window for 11.3 kHz tone bursts as an estimate of whether MET channel currents are impaired [47] (Fig. 5B, SP). Again, SP amplitude reduction was larger at higher (~70% at 16 kHz) than at lower or middle frequencies (~50% at 4-8 kHz) (the growth function is not shown as extra Figure). This assumption is supported by a failure to generate cochlear microphonic (CM) amplitudes upon increasing sound pressure levels in *Gnai3* cKO mice (Fig. 5C, CM). CM amplitudes are assumed to be proportional to the number of functional phasic MET currents from mainly basal-coil OHCs [48]. Overall, these findings support hampered activation of functional MET currents in high-frequency cochlear turns of *Gnai3* cKO mice to be causally related to hearing and hair bundle abnormalities.

In conclusion, a close structural/functional relationship between impaired stereocilia elongation upon *Gnai* deletion and impaired auditory responses is supported by (i) an overlap of hearing function deficit and Gα$_i$ expression patterns in either higher frequency (Gα$_{i3}$) or lower frequency cochlear regions (Gα$_{i2}$/Gα$_{i3}$), and (ii) impaired CAP, SP and CM function in *Gnai3* cKO towards higher frequencies.

Specific Gα$_{i2/i3}$ functions during maturation of IHC synapses

To obtain insight if the presumably impaired activation of MET currents might influence the maturation process of the hair cell phenotype in the high-frequency cochlear turn (*Gnai3* cKO) or in all cochlear turns (*Gnai2/i3* cKO) we inspected key biomarkers for hair cell maturation (Fig. 6). The motor protein prestin (Fig. 6A, left panel, green) and

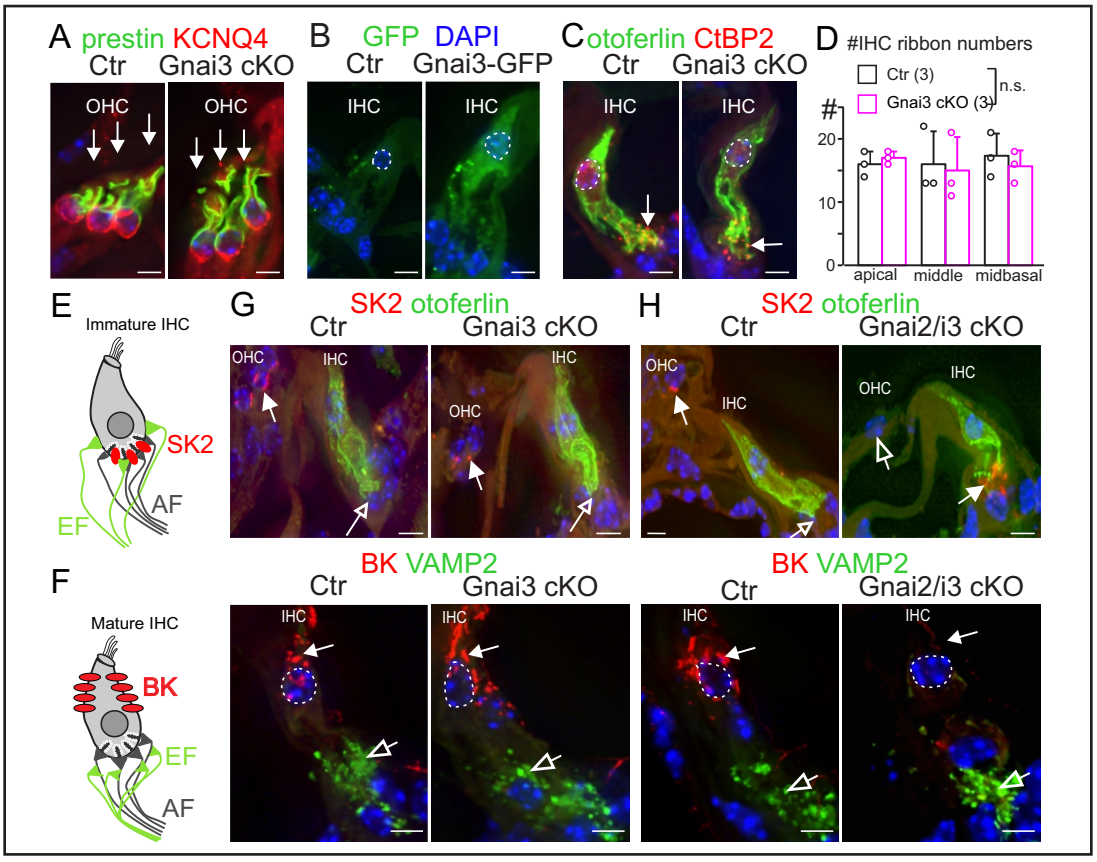

Fig. 6. Gα_{i2} and Gα_{i3} exhibit mutually redundant functions for IHC but not OHC differentiation. (A) Immunostaining of OHC functional markers KCNQ4 and prestin along the cochlear turns of 7- to 8-week-old control (Ctr) and *Gnai*3 cKO mice. No obvious differences of KCNQ4 (red) and prestin (green) expression are observed in OHCs from control and *Gnai*3 cKO mice as exemplified for high-frequency cochlear regions. One representative animal of n=5-7 is shown. (B) GFP expression in IHCs of 4-week-old *Gnai*3-GFP reporter mice confirming Gα_{i3} expression, whereas GFP is not detectable in IHCs of control littermates. One representative animal of n=2 is shown. (C) Immunostaining of CtBP2/RIBEYE (red) and otoferlin (green) in basal cochlear turn of 7- to 8-week-old control and *Gnai*3 cKO IHCs. No obvious differences in CtBP2/RIBEYE and otoferlin expression are observed between control and KO mice. One representative animal of n=2-4 is shown. (D) No significant difference in mean IHC ribbon counts±SD of 7- to 8-week-old control and *Gnai*3 cKO mice. Circles represent ribbon counts for individual animals (n=3 ears from 3 mice). (E, F) Schematic illustration of localization of SK2 and BK in immature (E) and mature (F) IHCs. (G) Normal otoferlin (green), BK (red), and VAMP 2 (green) immunostaining and expected lack of SK2 (red) in IHCs in basal cochlear turns of 7- to 8-week-old *Gnai*3 cKO mice (n=2-3 mice). (H) Immunostainings show immature SK2 expression and missing BK expression in 7- to 8-week-old *Gnai*2/i3 cKO IHCs (n=1-2 mice). (G, H) Otoferlin is used as IHC marker. VAMP2 stains efferent nerves. Circles indicate nuclei of IHCs. (G, H upper panel). Closed arrows indicate localization of SK2 in immature IHCs and open arrows indicate SK2 expression in OHCs. (G, H lower panel) Closed arrows indicate BK staining and open arrows indicate VAMP 2 staining. Scale bars, 10µm.

the voltage-gated K^+-channel KCNQ4 (Fig. 6A, left panel, red) are typically upregulated in OHCs before hearing onset [49-52] and remain expressed in the mature cochlea. In mature *Gnai3* mutants' OHCs both marker proteins were expressed as expected suggesting normal development (Fig. 6A, right panel). Analyzing GFP fluorescence in *Gnai3*-GFP reporter mice indicated that Gα_{i3} protein should be expressed in IHCs (Fig. 6B). Nevertheless, *Gnai3* cKO mice showed a normal expression profile of the Ca^{2+}-sensor protein otoferlin within the IHC [53] (Fig. 6C, green) with a regular distribution pattern (Fig. 6C, red) and no indication for

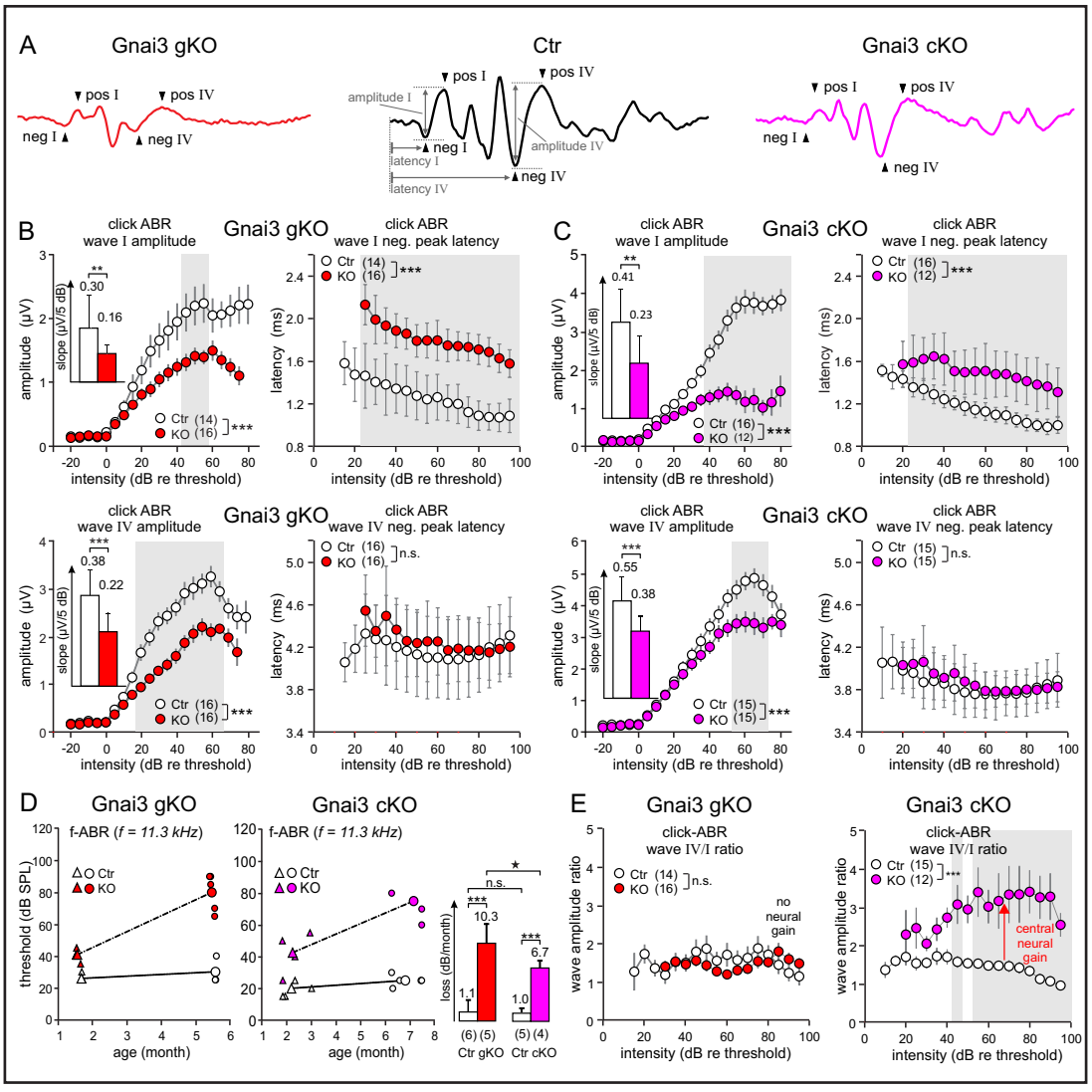

Fig. 7. ABR amplitudes, latencies, wave IV to wave I amplitude ratios, and ABR thresholds change over age in global and conditional *Gnai*3 KO mice. (A) Individual ABR waveform from control (Ctr, black) and *Gnai*3 KO (red and purple line) 1- to 3-month-old mice with indicated wave I and wave IV peak-to-peak amplitude (amplitude) and leading peak latency (latency). (B,C) ABR wave I (upper panels) and IV (lower panles) amplitude I/O functions (left panels) with slope (insets) and wave I and IV leading peak latency I/O function (right panels) for *Gnai*3 gKO (B), *Gnai*3 cKO (C) and respective control mice. Decrease of amplitudes, amplitude slope and increase of wave I latencies are evident in the KO mice (shaded areas, p< 0.05). (D) Age-related loss of ABR thresholds to 11.3 kHz stimuli for *Gnai*3 gKO and *Gnai*3 cKO mice at the age of 1-3 months (triangles) and 5-7 months (circles). Progression of threshold loss occurs in both KO mouse lines (dashed lines). The loss of ABR thresholds per month of age in *Gnai*3 KO mice significantly exceeded the loss in control mice (graph bars). The loss of ABR threshold per month was significantly larger in *Gnai*3 gKO mice than in *Gnai*3 cKO (star, p<0.05), and not significantly different between both control groups (n.s.). Thresholds for individual ears are denoted by small symbols. (E) ABR wave IV/I ratios for *Gnai*3 gKO, *Gnai*3 cKO and respective control mice. Significant elevation of wave IV/I ratios at middle to high stimulation levels is found only in *Gnai*3 cKO mice. Mean±SEM (straight error bars) or SD (error bars with caps) from 4 to 9 mice (number of ears in brackets).

an altered number (Fig. 6D) of CtBP2/RIBEYE protein-labeled ribbon structures, though the statistical conclusion may be limited by the small sample size. Furthermore, a characteristic feature of immature IHCs during normal development is the formation of an axosomatic

contact of efferent nerve fibers with the small conductance Ca^{2+}-activated K^+-channel type 2 (SK2) at the base of IHCs [54-56] (Fig. 6E). With hearing onset (P11-12), a reorganization of axosomatic efferent nerves on IHCs occurs that is characterized by downregulation of SK2 and upregulation of BK, both Ca^{2+}- and voltage-gated K^+-channels (Fig. 6F). BK channels carry $I_{K,f}$ currents that are essential to transform immature IHCs (exhibiting spontaneous Ca^{2+}-spikes) to mature functional cells that are then able to respond to sound [57, 58]. *Gnai3* cKO IHCs innervated by VAMP 2 positive efferent nerves mature normally, i.e. lacking SK2 at the base of otoferlin-positive cells (Fig. 6G, upper panel) and normal BK expression in supranuclear position on IHCs (Fig. 6G, lower panel). In contrast, in *Gnai2/i3* cKO IHCs an immature phenotype was observed along the entire tonotopic axis, characterized by a persistent expression of SK2 (Fig. 6H, upper panel) and a lack of BK expression (Fig. 6H, lower panel) at the basal pole of IHCs. Since *Gnai2* KO mice show no IHC maturation defects and IHCs from *Gnai3* cKO mice develop normally in spite of hair bundle defects, whereas IHCs from *Gnai2/i3* cKO remain in an immature stage, we conclude that $G\alpha_{i2}$ or $G\alpha_{i3}$ function is required for final maturation of IHC synapses prior to hearing onset.

Function of $G\alpha_{i3}$ in the central auditory pathway correlates with its expression in satellite cells and brainstem auditory nuclei

Although IHCs mature normally in *Gnai3* KO mice their hair bundles are defective (see Fig. 3B-E) and functionally impaired (see Fig. 1C,D,F), and the cochlear output is diminished (see Fig. 5). Therefore, we were interested whether central auditory processing is also affected and studied supra-threshold ABR wave amplitudes, which reflect the summed activity of the auditory nerve independent of OHC contribution to hearing thresholds.

Whereas *Gnai2* cKO mice showed normal early (ABR wave I) and late (ABR wave IV) amplitudes and latencies in response to click sound stimuli (see online suppl. material, suppl. Fig. 3), supra-threshold ABR wave I amplitudes were significantly reduced in both *Gnai3* gKO (Fig. 7A and B) and *Gnai3* cKO mice (Fig. 7A and C) in comparison to controls. In addition, the slopes of the amplitude growth functions were significantly weaker as compared to controls (Fig. 7B and C, inset left panels). Moreover, a significant delay of the leading peak of ABR wave I that recovered towards ABR wave IV became apparent (Fig. 7B and C, right panels). Reduced amplitude and response delay are consistent with the observed diminished cochlear output as we think is a consequence of impaired activation of IHC MET channels. This was accompanied by an accelerated threshold loss over age observed in ABRs at a stimulation frequency of 11.3 kHz (and thresholds of DPOAE at f2=11.3 kHz, not shown) as seen in individual mice at different age, i.e. 1.5-3 months vs. 5.4-7.5 months (Fig. 7D). The rate of loss of ABR thresholds per month of age in *Gnai3* KO mice exceeded significantly the minor loss seen in control mice (Fig. 7D, bar graphs). Furthermore, the progression of ABR threshold loss was significantly stronger in global *Gnai3* KO mice when compared to mice with conditional *Gnai3* deletion (Fig. 7D, bar graph) while no significant difference was found when comparing the progression for the respective controls (Fig. 7D, bar graph).

Strikingly, the amplitude of ABR wave IV was disproportionally elevated in comparison to ABR wave I in *Gnai3* cKO mice but not in *Gnai3* gKO (Fig. 7E), indicating that conditional deletion of *Gnai3* mainly restricted to the inner ear preserves a capacity to generate neural gain, while this function is mostly lost in global *Gnai3* KO mice. In *Gnai2* KO mice showing normal hearing and in *Gnai2/i3* cKO being almost deaf this effect was not further analyzed. The different capabilities of global and conditional *Gnai3* KO to generate central neural gain suggested that distinct $G\alpha_{i3}$ expression patterns might be causally involved in the progression of the deviating functional phenotypes. Isoform-specific antibodies detected $G\alpha_{i3}$ proteins in the brainstem and cerebellar tissues from control but not from *Gnai3* gKO mice (see online suppl. material, suppl. Fig. 4, upper panel), whereas in the same tissues $G\alpha_{i1/i2}$ immunoreactivity was unaffected (see online suppl. material, suppl. Fig. 4, middle panel). We next searched for differences in the expression pattern of $G\alpha_{i3}$ between *Gnai3* gKOs and *Gnai3* cKOs in retrocochlear regions possibly involved in neural gain generation at the level of the auditory nerve or its target neurons in the cochlear nucleus [59, 60].

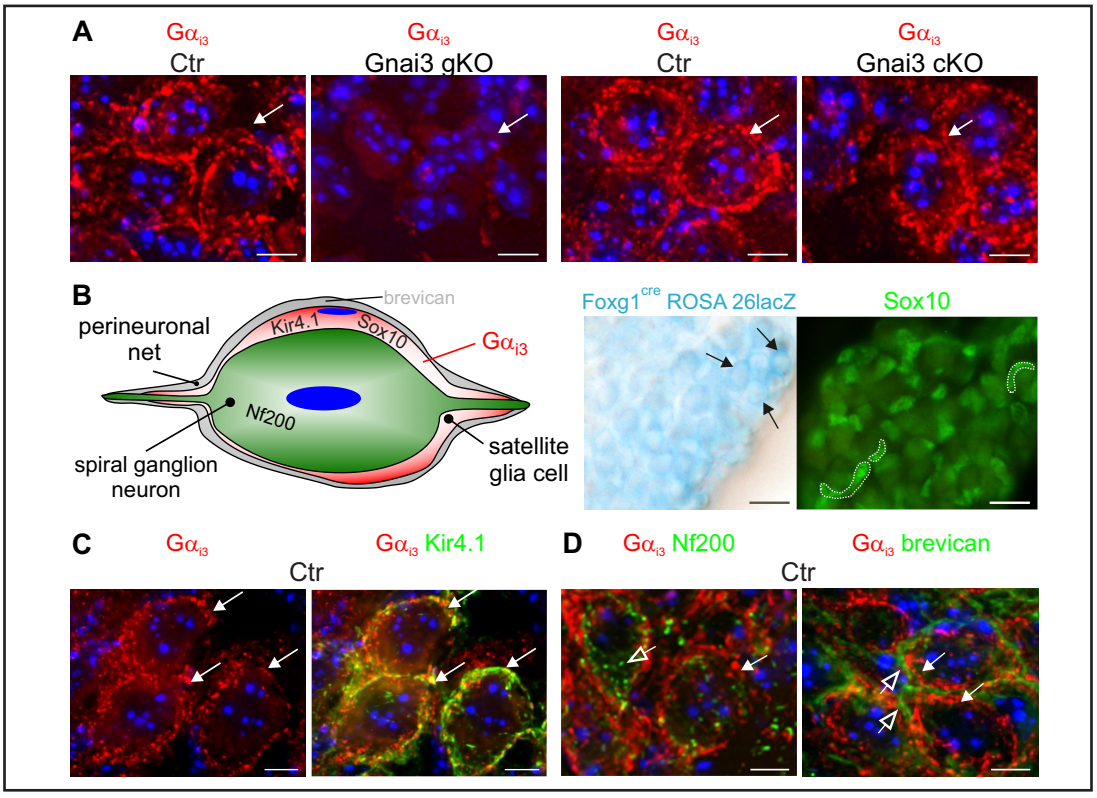

Fig. 8. Expression of Gα$_{i3}$ in the spiral ganglion. (A) Sections through the spiral ganglion stained with Gα$_{i3}$ antibodies reveal its presence in control (Ctr) and *Gnai*3 cKO mice but not in *Gnai*3 gKO mutants. One representative animal of n=2 is shown. Scale bars, 5µm (B) Schematic illustration of the expected Nf200, Kir4.1, Sox10, brevican, and Gα$_{i3}$ immunoreactivity in the soma of a single spiral ganglion neuron and the ensheathing satellite (glia) cell, and the surrounding perineural net matrix. Lac Z staining of Foxg1$^{cre/+}$ROSA 26 reveals activity of Cre in the cytoplasm of spiral ganglion neurons (middle panel, some somas are indicated with arrows) but not in neighboring Sox10-labelled satellite cells (right panel, some cells are indicated with white outlines). Scale bars, 15µm. One representative animal of n=2 is shown. (C, D) Sections through the spiral ganglion co-labelled with Gα$_{i3}$ and Kir4.1 antibodies confirm its presence in satellite cells surrounding Nf200 positive spiral ganglion neurons. Gα$_{i3}$ itself is surrounded by the perineuronal marker brevican. Scale bars, 5µm. One representative animal of n=2-5 is shown.

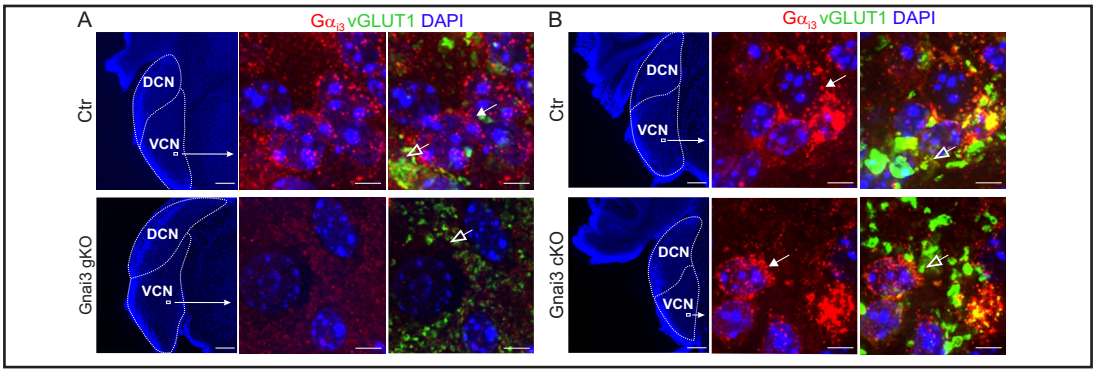

Fig. 9. Gα$_{i3}$ and vGLUT1 expression in the ventral cochlear nucleus. (A,B) Left panels: Overview of cross sections showing dorsal (DCN) and ventral (VCN) cochlear nucleus of *Gnai*3 gKO (A) and *Gnai*3 cKO (B) and corresponding controls (Ctr). Scale bars 200µm. Middle and right panels: stained with Gα$_{i3}$-specific antibodies (red) and the vesicular-glutamate-transporter-1 (vGLUT1, green). Note the absence of Gα$_{i3}$ labeling contacted by vGLUT1 in *Gnai*3 gKO (A) but not cKO (B). One representative animal of n=2 is shown. Scale bars 5µm.

At the level of the spiral ganglion neurons (SGN) $G\alpha_{i3}$ immunoreactivity was absent in *Gnai3* gKO but not in *Gnai3* cKO mice (Fig. 8A). Also in target neurons of the auditory nerve in the cochlear nucleus (e.g. the bushy cells in the ventral cochlear nucleus, VCN), which are identified through vGLUT1 positive presynaptic contacts (Fig. 9, green) [61], $G\alpha_{i3}$ antibody staining was detected in *Gnai3* cKO (Fig. 9B, red) but not in *Gnai3* gKO mice (Fig. 9A, red). Moreover, preliminary findings revealed reduced vGLUT1 staining intensity in *Gnai3* gKOs (Fig. 9A, green) in comparison to *Gnai3* cKO mice and control mice (Fig. 9B, green). As previously described reduced vGLUT1 expression goes along with reduced activity [61], we suggest differences in vGLUT1 activity of auditory nerves between both *Gnai3* mutants.

To search for additional differences between *Gnai3* gKO and *Gnai3* cKO mice we compared the expression pattern of $G\alpha_{i3}$ with that of the Cre activity generated by the Foxg1$^{cre/+}$ line used to generate *Gnai3* cKO mice. Lac Z staining of Foxg1$^{cre/+}$ROSA 26 animals showed Cre activity in the ball-shaped SGNs (Fig. 8B, middle panel) which correspond to the previously described expression of Foxg1 [27]. $G\alpha_{i3}$ expression was assigned to the bean-shaped supporting satellite cells, which were characterized by Sox10 expression (Fig. 8B, right panel) and colabelling with the marker Kir4.1 [62, 63] (Fig. 8B and C) surrounding the Nf200 positive SGNs (Fig. 8B and D, left panel). Furthermore, $G\alpha_{i3}$ expression itself was encircled by the perineuronal net marker brevican [64] (Fig. 8B and D, right panel). Importantly, expression of $G\alpha_{i3}$ in satellite cells is evident in *Gnai3* cKO but not in *Gnai3* gKO mice and hence could contribute to auditory neural gain only seen in *Gnai3* cKO.

Taken together, our findings have various implications on the role of $G\alpha_i$ proteins as regulators of auditory functions and can be summarized by four key observations (Fig. 10). (1) Hair bundles in low-frequency regions are shaped by $G\alpha_{i2}$ and/or $G\alpha_{i3}$ whereas their correct formation in high-frequency regions only depends on $G\alpha_{i3}$ (Fig. 10A). (2) At least one $G\alpha_i$ isoform is required to trigger the final maturation of IHC synapses (Fig. 10B). (3) In low-frequency regions the deletion of either $G\alpha_{i2}$ or $G\alpha_{i3}$ has no hearing phenotype, whereas in high-frequency regions $G\alpha_{i3}$ is required for appropriate hearing (Fig. 10C). (4) Expression of $G\alpha_{i3}$ in satellite cells of the cochlea and/or auditory neurons in the brainstem associates with neural gain adjustment (Fig. 10D).

Discussion

The present study unravels specific auditory functions of different $G\alpha_i$ proteins, the binding partners of Gpsm2, which are known as evolutionary highly conserved determinants of cell polarity, asymmetric cell division, or planar cell polarity [11, 42]. The present data provide evidence to discriminate between so far elusive functions of $G\alpha_{i2}$ and $G\alpha_{i3}$ for (1) shaping polarity and length of hair bundles in different cochlear regions, and (2) also uncover new functionally relevant actions of $G\alpha_{i2}$ and $G\alpha_{i3}$ for final differentiation of inner hair cell (IHC) synapses, and (3) suggest $G\alpha_{i3}$ to be important for central auditory adaptation processes.

$G\alpha_{i2}$ and $G\alpha_{i3}$ shape hair bundles

Using various *Gnai* mutant mouse lines we demonstrate that deficiency for $G\alpha_{i3}$ but not $G\alpha_{i2}$ produces high-frequency hearing loss, whereas the absence of both isoforms results in profound deafness resembling the phenotype seen in *Gpsm2* mouse mutants [19, 23].

Lower numbers and reduced elongation of stereocilia in high frequency cochlear turns in outer hair cells (OHCs) of *Gnai3* cKO mice and stereociliary elongation defects in IHC in basal turns [19] correlated with the deficiency for *Gnai3* in high frequency cochlear regions and high frequency hearing threshold loss. In contrast, due to an overlapping expression profile of $G\alpha_{i2}$ and $G\alpha_{i3}$ proteins we observed reduced numbers and impaired elongation of stereocilia together with low-frequency hearing threshold loss exclusively in the *Gnai2/i3* cKO mice which are deficient for both proteins. These findings uncover an unexpected difference of $G\alpha_{i2}$ and $G\alpha_{i3}$ functions for shaping size and length of hair cell stereociliary bundles specifically along the tonotopic axis and suggest selective $G\alpha_{i3}$ functions for hearing

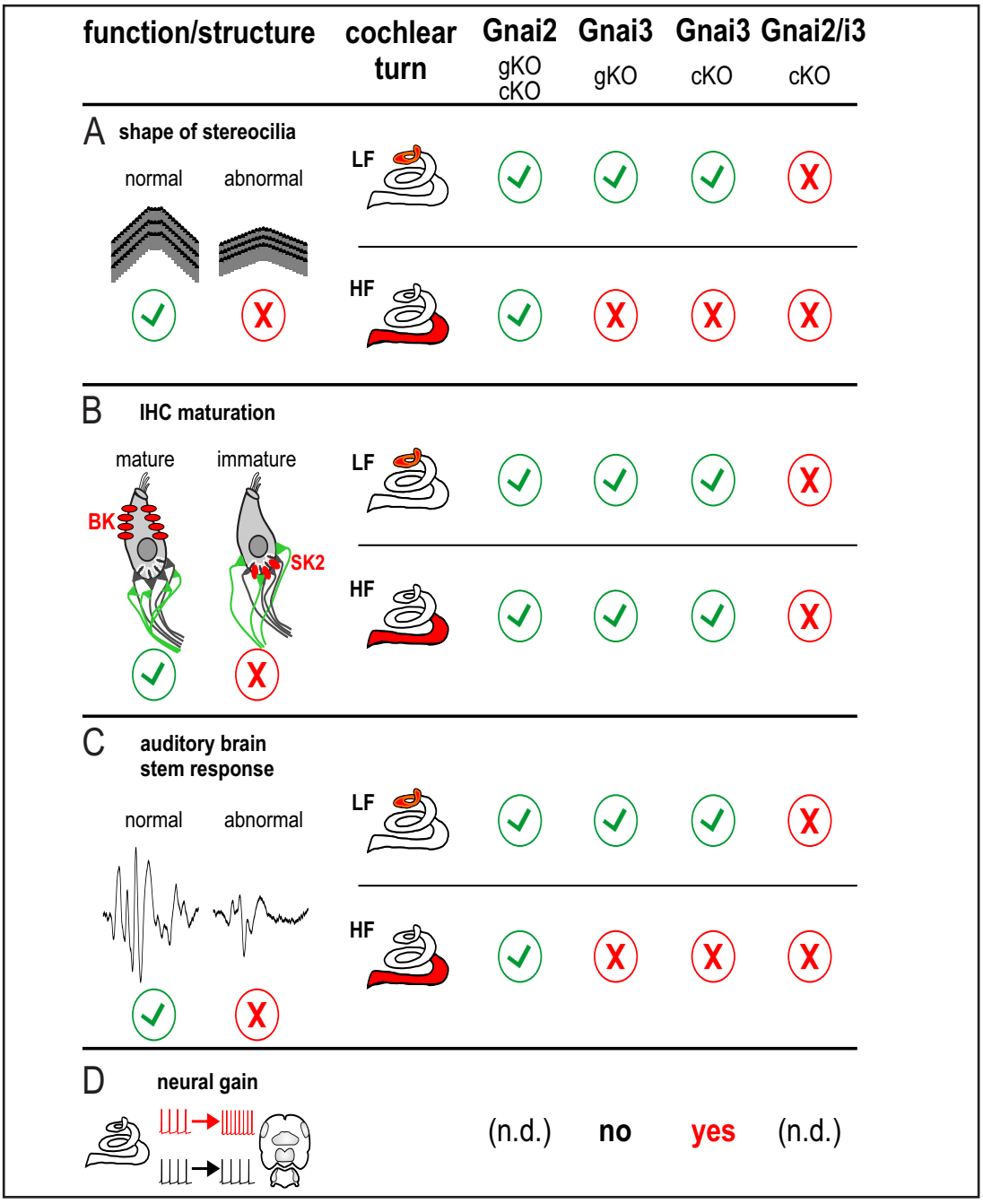

Fig. 10. Schematic illustration of supposed roles of $G\alpha_{i2}$ and $G\alpha_{i3}$ for hearing. (A) Hair bundles in low-frequency cochlear regions are shaped by $G\alpha_{i2}$ and $G\alpha_{i3}$ activity and hair bundles in high-frequency cochlear regions are shaped by specific activity of $G\alpha_{i3}$ that cannot be replaced by $G\alpha_{i2}$. (B) During the maturation process the reorganization of the axosomatic efferent nerves is described by the downregulation of SK2 and upregulation of BK channels. $G\alpha_{i2}$ and $G\alpha_{i3}$ exhibit mutual redundant activity to trigger the final maturation of IHC synapses, whereas upon deletion of both $G\alpha_i$ proteins IHCs remain in an immature stage characterized by a sustained SK2 expression and a failure of BK upregulation. (C) For hearing in low-frequency regions expression of either $G\alpha_{i2}$ or $G\alpha_{i3}$ is indispensable, whereas in high-frequency regions $G\alpha_{i3}$ expression is crucial for proper hearing. (D) Central neural gain adjustment in response to impaired auditory input is presumably shaped by $G\alpha_{i3}$ activity in satellite cells or brainstem auditory neurons, as $G\alpha_{i3}$ is absent in *Gnai*3 gKO but not in *Gnai*3 cKO mice in these cells. n.d., not determined. LF, low-frequency. HF, high-frequency.

low and high pitch sounds. In this context the existence of frequency-specific complexes of either $G\alpha_{i2}$ or $G\alpha_{i3}$ together with actin regulatory proteins (such as espin, radixin, TRIOBP or twinfilin) [65-67] or with hair cell-specific myosins (Myosin 1c, 3a, 6, 7a and 15a) [65, 68] or proteins such as Eps8 (actin-binding protein epidermal growth factor receptor pathway substrate 8) [55, 69], whirlin [19] and proteins associated with the mechanoelectrical transduction (MET) [70] may be considered.

The failure of proper activation of functionally intact MET may be explained through structural abnormalities of stereocilia in *Gnai3* KO mice, such as shorter hair bundles. Indeed, we have several implications that MET are functional: (i) normal slopes but reduced CAP amplitudes in *Gnai3* cKO mice point to functional MET currents [71] (ii) reduced summated potential (SP) amplitudes indicating functional MET currents although the activation of those seems to be hampered [47] (iii) the deficient growth of cochlear microphonics (CM) typically seen upon insufficient responses of MET currents to sound caused by an inappropriate activation of the MET channels [72] and (iv) the shallower slopes of the amplitude growth functions of early and late ABR waves at moderate sound intensities observed in global and conditional *Gnai3* KO mice point to reduced sensitivity to sound [73]. The overall findings thus suggest a failure of functionally intact MET activation in *Gnai3* KO mice following e.g. inappropriate coupling of shorter or disorganized stereocilia to the tectorial membrane. Reduced length of stereocilia despite normal biophysical properties of MET currents is also discussed for Eps8 mutants [55]. Eps8 shapes stereocilia length together with Usher protein candidates such as whirlin or myosin 15 along the entire tonotopic axis [74]. Deletion of the Eps8L2, a member of the Eps8-like protein family, causes deafness [55, 69] similarly to *Gnai2/i3* cKO. Strikingly, the deletion of Eps8 induced progressive high-frequency hearing loss [75] similar to the phenotype observed here in *Gnai3* KO mice. Further studies will clarify whether $G\alpha_i$ protein expression and/or signaling depends on Eps8 or *vice versa*. Moreover, it remained open in which signaling pathways $G\alpha_i$ integrates in the inner ear. Aside from classical GPCR-driven canonical pathways non-canonical mechanisms should be considered in future studies.

$G\alpha_{i2}$ and $G\alpha_{i3}$ trigger maturation of IHC synapses

IHCs of *Gnai2/i3* cKO mice remain immature along the entire tonotopic axis as judged from a failure to upregulate BK and downregulate SK2 channels. Since *Gnai3* mutants develop a normal post-hearing IHC structural phenotype, the impairment of stereocilia elongation *per se* is unlikely the cause of the developmental block of IHC maturation. Deafness by itself does not prevent IHC maturation of *Gnai2/i3* cKO mice, as can be concluded from situations of hereditary deafness that do not prevent proper IHC maturation; for example the absence of thyroid hormone leads to deafness, but IHCs gradually develop after 2 months [76-78], whereas IHC maturation is still absent in 4- to 5-month-old *Gnai2/i3* cKO mice. The immature IHC phenotype of *Gnai2/i3* cKO mice may rather be considered in the context of a redundant $G\alpha_{i2}/G\alpha_{i3}$ activity that acts together with myosin 6 e.g. on pruning of connected fibers. Accordingly a timely elimination of axosomatic efferent contacts [54-56], coincides with the initiation of biophysical maturation in IHCs [79] (see for a review [58]). Myosin 6 mutants show not only a defective structural integrity of the hair bundle but also an impaired post-hearing IHC maturation that includes the failure to properly target BK channels [80, 81], similar to *Gnai2/i3* cKO.

$G\alpha_{i3}$ is essential for central auditory processing

An unexpected finding was a reduced compensatory neural gain in the *Gnai3* gKO but not in the *Gnai3* cKO mice that came along with a significantly accelerated worsening of hearing thresholds over age. For the auditory system, it was shown that the peripheral loss of response to sensory stimuli due to traumatic events, aging processes or genetic defects among others triggers central gain adjustment in order to re-stabilize the network through a disproportional elevation of the neuronal firing rate [31, 82, 83]. How target neurons of auditory nerve fibers, likely to be present in the dorsal [59] or ventral [84] cochlear nucleus

(DCN, VCN), sense nerve deprivation and re-stabilize their firing rate proportional to sensory decline is entirely elusive.

The finding that central compensation fails in *Gnai3* gKO but not in *Gnai3* cKO, despite comparable hearing threshold deficits, is surprising. It is tempting to speculate that $G\alpha_{i3}$ expressing auditory neurons that may correspond to target cells of auditory nerves *via* their vGLUT1 positive contacts [85] may participate in generation of compensating central hyperactivity. Indeed, Gα-Gβγ signaling has been shown to modulate basic G protein-activated K^+-channel GIRK [86] in response to e.g. $GABA_BR$ mediated (GABA "spillover") activation from neighboring sites and thereby triggers elevated firing rates through shunting of excitatory currents [87]. Interestingly, following noise exposure elevated firing rates in the cochlear nucleus (CN) are accompanied by a modification of $GABA_BR$ [88, 89]. In this context preliminary findings of lower vGLUT1 immunoreactivity in *Gnai3* gKO than *Gnai3* cKO mice may be indicative for less active transmitter release sites, as previously suggested [61]. Additionally, the absence of $G\alpha_{i3}$ expression in satellite cells of the cochlea in global but not conditional *Gnai3* mutants (Fig. 8A) may lead to a differential excitability of cochlear neuronal cells as has been observed for the brain [90, 91]. Indeed, dysfunction of satellite cells has been shown to accelerate hearing loss over age and delays ABR wave I responses in high-frequency hearing loss [92] as seen here for *Gnai3* KO.

$G\alpha_i$ proteins and in particular the $G\alpha_{i3}$ isoform have been previously linked to control asymmetric cell division and hair cell bundle polarity in the inner ear [16, 17, 19, 23]. Beyond that, our present findings indicate redundant functions of $G\alpha_{i2}$ and $G\alpha_{i3}$ for final maturation of synapses and low frequency hearing, whereas $G\alpha_{i3}$ is indispensable for basal cochlea hair bundle shaping, high frequency hearing, and homeostatic excitability changes in the brain. As a consequence, $G\alpha_i$ cell functions are not only pathophysiologically important for hearing, but should also be considered in the context of novel functions for the sensory synapse and neuronal differentiation processes.

Conclusion

From invertebrates to mammals, $G\alpha_i$ proteins are involved in regulation of mitotic spindle dynamics, cell division, polarity, growth, and differentiation. We show for the sensory cells in the cochlea that the action of $G\alpha_i$ members is not limited to cilia movements or regulation of mitotic spindle dynamics in early development, but that distinct isoforms differentially account for early and later developmental steps. In particular $G\alpha_i$ proteins (*i*) shape stereociliary bundles isoform-specifically, *(ii)* act on differentiation of synapses during critical rewiring periods and *(iii)* allow for central adaptive neural gain responses.

Abbreviations

ABR (auditory brainstem response); AGS (activators of G-protein signaling); BK (Ca^{2+}- and voltage-activated K^+-channels of the BK type); CAP (compound action potential); CN (cochlear nucleus); CM (cochlear microphonic potential); cKO (conditional deletion); dB (decibel); DCN (dorsal cochlear nucleus); DPOAE (distortion product otoacoustic emissions); ES (embryonic stem cells); Eps8 (actin-binding protein epidermal growth factor receptor pathway substrate 8); f1 (DPOAE primary tone 1 frequency); f2 (DPOAE primary tone 2 frequency); GFP (green fluorescent protein); gKO (global deletion); Gα (α subunit of G-proteins); GDI (guanine nucleotide dissociation inhibitor); GIRK (G protein-coupled inwardly-rectifying potassium channels); Gnai (gene coding for Gα subunit); GPCR (G-protein-coupled receptors); Gpsm2 (G protein signaling modulator 2); IHC (inner hair cells); I/O (input/output function); Kir4.1 (inward rectifying potassium channel); MET (mechanoelectrical transduction); Nf200 (neurofilament 200); n.s., not (significant); OHC (outer hair cell(s)); PTX (Pertussis Toxin); SD (standard deviation); SEM (standard error of the mean); SGN (spiral ganglion neuron); SK2 (small conductance Ca^{2+}-activated K^+-channel type 2); SP (summation potential); SPL (sound pressure level); VAMP 2 (vesicle-associated

membrane protein 2); VCN (ventral cochlear nucleus); vGLUT 1 (vesicular glutamate transporter 1).

Acknowledgements

We thank Renate Riehle for excellent assistance, the personnel of the Bordeaux Imaging Center (BIC, a service unit of the CNRS-INSERM & Bordeaux Univ., supported by the French National Research Agency (ANR-10-INSB-04, "Investments for the Future"), and the LabEX BRAIN ANR-10-LABX-43. This study was supported by grants from the Deutsche Forschungsgemeinschaft (KN316/4-1, and KN316/12-1 to MK; FOR 729, project A2, SFB 612, project A8, and Nu53/13-1 to BN; FOR 729, project A6 to KP), from DAAD (Project ID 57390169) to BN, ICePhA grant (Z project: ICePhA mouse clinic) to BN, the Hahn Stiftung (Index AG), the INSERM and the ANR GHearAct (ANR-14-CE13-0013-01) to MM, and the Intramural Research Program of the NIH (project Z01-ES-101643) to LB. B.N. conceived the project; S.B.-H., M.K., M.M., B.N., L.R. coordinated the study and designed research; S.B.-H., K.B., C.C., A.F., I.G., C.H., S.C.L., V.L., M.M., S.M., A.N., K.N., R.P.P, L.R. performed research; K.P., L.B., T.S. contributed reagents; S.B.-H., S.C.L., C.C., A.F., I.G., M.K., V.L., M.M., B.N., R.P.P, L.R. analyzed data; S.B.-H., I.G., M.K., V.L., M.M., B.N., L.R., T.S., W.S., U.Z. wrote the paper.

Disclosure Statement

The authors declare no competing financial interest.

References

1 Neves SR, Ram PT, Iyengar R: G protein pathways. Science 2002;296:1636-1639.
2 Rosenbaum DM, Rasmussen SG, Kobilka BK: The structure and function of G-protein-coupled receptors. Nature 2009;459:356-363.
3 Wong YH, Federman A, Pace AM, Zachary I, Evans T, Pouyssegur J, Bourne HR: Mutant a subunits of G_{i2} inhibit cyclic AMP accumulation. Nature 1991;351:63-65.
4 Xiao RP, Avdonin P, Zhou YY, Cheng H, Akhter SA, Eschenhagen T, Lefkowitz RJ, Koch WJ, Lakatta EG: Coupling of b2-adrenoceptor to G_i proteins and its physiological relevance in murine cardiac myocytes. Circ Res 1999;84:43-52.
5 Pines M, Santora A, Gierschik P, Menczel J, Spiegel A: The inhibitory guanine nucleotide regulatory protein modulates agonist-stimulated cAMP production in rat osteosarcoma cells. Bone Miner 1986;1:15-26.
6 Culurgioni S, Mapelli M: Going vertical: functional role and working principles of the protein Inscuteable in asymmetric cell divisions. Cell Mol Life Sci 2013;70:4039-4046.
7 Blumer JB, Lanier SM: Activators of G protein signaling exhibit broad functionality and define a distinct core signaling triad. Mol Pharmacol 2014;85:388-396.
8 Malbon CC: G proteins in development. Nat Rev Mol Cell Biol 2005;6:689-701.
9 Morin X, Bellaïche Y: Mitotic spindle orientation in asymmetric and symmetric cell divisions during animal development. Dev Cell 2011;21:102-119.
10 Siller KH, Doe CQ: Spindle orientation during asymmetric cell division. Nat Cell Biol 2009;11:365-374.
11 Blumer JB, Oner SS, Lanier SM: Group II activators of G-protein signalling and proteins containing a G-protein regulatory motif. Acta Physiol (Oxf) 2012;204:202-218.
12 Williams SE, Ratliff LA, Postiglione MP, Knoblich JA, Fuchs E: Par3-mInsc and Ga_{i3} cooperate to promote oriented epidermal cell divisions through LGN. Nat Cell Biol 2014;16:758-769.
13 Mochizuki N, Cho G, Wen B, Insel PA: Identification and cDNA cloning of a novel human mosaic protein, LGN, based on interaction with G alpha i2. Gene 1996;181:39-43
14 Sato M, Blumer JB, Simon V, Lanier SM: Accessory proteins for G proteins: partners in signaling. Annu Rev Pharmacol Toxicol 2006;46:151-187.

15 McCudden CR, Willard FS, Kimple RJ, Johnston CA, Hains MD, Jones MB, Siderovski DP: Ga selectivity and inhibitor function of the multiple GoLoco motif protein GPSM2/LGN. Biochimi Biophys Acta 2005;1745:254-264.
16 Ezan J, Lasvaux L, Gezer A, Novakovic A, May-Simera H, Belotti E, Lhoumeau AC, Birnbaumer L, Beer-Hammer S, Borg JP, Le Bivic A, Nürnberg B, Sans N, Montcouquiol M: Primary cilium migration depends on G-protein signalling control of subapical cytoskeleton. Nat Cell Biol 2013;15:1107-1115.
17 Tarchini B, Jolicoeur C, Cayouette M: A molecular blueprint at the apical surface establishes planar asymmetry in cochlear hair cells. Dev Cell 2013;27:88-102.
18 Hamzeh AR, Nair P, Mohamed M, Saif F, Tawfiq N, Al-Ali MT, Bastaki F: A novel nonsense GPSM2 mutation in a Yemeni family underlying Chudley-McCullough syndrome. Eur J Med Genet 2016;59:337-341.
19 Mauriac SA, Hien YE, Bird JE, Carvalho SD, Peyroutou R, Lee SC, Moreau MM, Blanc JM, Geyser A, Medina C, Thoumine O, Beer-Hammer S, Friedman TB, Ruttiger L, Forge A, Nürnberg B, Sans N, Montcouquiol M: Defective Gpsm2/Galphai3 signalling disrupts stereocilia development and growth cone actin dynamics in Chudley-McCullough syndrome. Nat Commun 2017;8:14907.
20 Doherty D, Chudley AE, Coghlan G, Ishak GE, Innes AM, Lemire EG, Rogers RC, Mhanni AA, Phelps IG, Jones SJ, Zhan SH, Fejes AP, Shahin H, Kanaan M, Akay H, Tekin M, Consortium FC, Triggs-Raine B, Zelinski T: GPSM2 mutations cause the brain malformations and hearing loss in Chudley-McCullough syndrome. Am J Hum Genet 2012;90:1088-1093.
21 Walsh T, Shahin H, Elkan-Miller T, Lee MK, Thornton AM, Roeb W, Abu Rayyan A, Loulus S, Avraham KB, King MC, Kanaan M: Whole exome sequencing and homozygosity mapping identify mutation in the cell polarity protein GPSM2 as the cause of nonsyndromic hearing loss DFNB82. Am J Hum Genet 2010;87:90-94.
22 Yariz KO, Walsh T, Akay H, Duman D, Akkaynak AC, King MC, Tekin M: A truncating mutation in GPSM2 is associated with recessive non-syndromic hearing loss. Clin Genet 2012;81:289-293.
23 Tarchini B, Tadenev AL, Devanney N, Cayouette M: A link between planar polarity and staircase-like bundle architecture in hair cells. Development 2016;143:3926-3932.
24 Jiang M, Spicher K, Boulay G, Martin-Requero A, Dye CA, Rudolph U, Birnbaumer L: Mouse gene knockout and knockin strategies in application to a subunits of Gi/Go family of G proteins. Methods Enzymol 2002;344:277-298.
25 Plummer NW, Spicher K, Malphurs J, Akiyama H, Abramowitz J, Nürnberg B, Birnbaumer L: Development of the mammalian axial skeleton requires signaling through the Gai subfamily of heterotrimeric G proteins. Proc Natl Acad Sci U S A 2012;109:21366-21371.
26 Leiss V, Flockerzie K, Novakovic A, Rath M, Schonsiegel A, Birnbaumer L, Schurmann A, Harteneck C, Nürnberg B: Insulin secretion stimulated by L-arginine and its metabolite L-ornithine depends on Ga_{i2}. Am J Physiol Endocrinol Metab 2014;307:E800-812.
27 Hébert JM, McConnell SK: Targeting of cre to the Foxg1 (BF-1) locus mediates loxP recombination in the telencephalon and other developing head structures. Dev Biol 2000;222:296-306.
28 Skokowa J, Ali SR, Felda O, Kumar V, Konrad S, Shushakova N, Schmidt RE, Piekorz RP, Nürnberg B, Spicher K, Birnbaumer L, Zwirner J, Claassens JW, Verbeek JS, van Rooijen N, Kohl J, Gessner JE: Macrophages induce the inflammatory response in the pulmonary Arthus reaction through Ga_{i2} activation that controls C5aR and Fc receptor cooperation. J Immunol 2005;174:3041-3050.
29 Gohla A, Klement K, Piekorz RP, Pexa K, vom Dahl S, Spicher K, Dreval V, Haussinger D, Birnbaumer L, Nürnberg B: An obligatory requirement for the heterotrimeric G protein G_{i3} in the antiautophagic action of insulin in the liver. Proc Natl Acad Sci U S A 2007;104:3003-3008.
30 Rudolph U, Finegold MJ, Rich SS, Harriman GR, Srinivasan Y, Brabet P, Boulay G, Bradley A, Birnbaumer L: Ulcerative colitis and adenocarcinoma of the colon in G alpha i2-deficient mice. Nature Genetics 1995;10:143-150.
31 Zuccotti A, Kuhn S, Johnson SL, Franz C, Singer W, Hecker D, Geisler HS, Köpschall I, Rohbock K, Gutsche K, Dlugaiczyk J, Schick B, Marcotti W, Rüttiger L, Schimmang T, Knipper M: Lack of brain-derived neurotrophic factor hampers inner hair cell synapse physiology, but protects against noise-induced hearing loss. J Neurosci 2012;32:8545-8553.
32 Chumak T, Rüttiger L, Lee SC, Campanelli D, Zuccotti A, Singer W, Popelar J, Gutsche K, Geisler HS, Schraven SP, Jaumann M, Panford-Walsh R, Hu J, Schimmang T, Zimmermann U, Syka J, Knipper M: BDNF in lower

brain parts modifies auditory fiber activity to gain fidelity but increases the risk for generation of central noise after injury. Mol Neurobiol 2015;53:5607-5627.

33 Engel J, Braig C, Rüttiger L, Kuhn S, Zimmermann U, Blin N, Sausbier M, Kalbacher H, Münkner S, Rohbock K, Ruth P, Winter H, Knipper M: Two classes of outer hair cells along the tonotopic axis of the cochlea. Neuroscience 2006;143:837-849.

34 Winter H, Rüttiger L, Müller M, Kuhn S, Brandt N, Zimmermann U, Hirt B, Bress A, Sausbier M, Conscience A, Flamant F, Tian Y, Zuo J, Pfister M, Ruth P, Löwenheim H, Samarut J, Engel J, Knipper M: Deafness in TRb mutants is caused by malformation of the tectorial membrane. J Neurosci 2009;29:2581-2587.

35 Davies S, Forge A: Preparation of the mammalian organ of Corti for scanning electron microscopy. J Microscopy 1987;147:89-101.

36 Knipper M, Gestwa L, Ten Cate WJ, Lautermann J, Brugger H, Maier H, Zimmermann U, Rohbock K, Köpschall I, Wiechers B, Zenner HP: Distinct thyroid hormone-dependent expression of TrKB and $p75^{NGFR}$ in nonneuronal cells during the critical TH-dependent period of the cochlea. J Neurobiol 1999;38:338-356.

37 Singer W, Zuccotti A, Jaumann M, Lee SC, Panford-Walsh R, Xiong H, Zimmermann U, Franz C, Geisler HS, Köpschall I, Rohbock K, Varakina K, Verpoorten S, Reinbothe T, Schimmang T, Rüttiger L, Knipper M: Noise-induced inner hair cell ribbon loss disturbs central arc mobilization: a novel molecular paradigm for understanding tinnitus. Mol Neurobiol 2013;47:261-279.

38 Hahn H, Müller M, Löwenheim H: Whole organ culture of the postnatal sensory inner ear in simulated microgravity. J Neurosci Methods 2008;171:60-71.

39 Tan J, Rüttiger L, Panford-Walsh R, Singer W, Schulze H, Kilian SB, Hadjab S, Zimmermann U, Köpschall I, Rohbock K, Knipper M: Tinnitus behavior and hearing function correlate with the reciprocal expression patterns of BDNF and Arg3.1/arc in auditory neurons following acoustic trauma. Neuroscience 2007;145:715-726.

40 Winter H, Braig C, Zimmermann U, Engel J, Rohbock K, Knipper M: Thyroid hormone receptor alpha1 is a critical regulator for the expression of ion channels during final differentiation of outer hair cells. Histochem Cell Biol 2007;128:65-75.

41 Winter H, Braig C, Zimmermann U, Geisler HS, Franzer JT, Weber T, Ley M, Engel J, Knirsch M, Bauer K, Christ S, Walsh EJ, McGee J, Köpschall I, Rohbock K, Knipper M: Thyroid hormone receptors TRa1 and TRb differentially regulate gene expression of Kcnq4 and prestin during final differentiation of outer hair cells. J Cell Sci 2006;119:2975-2984.

42 Ezan J, Montcouquiol M: Revisiting planar cell polarity in the inner ear. Semin Cell Develop Biol 2013;24:499-506.

43 Zampini V, Johnson SL, Franz C, Lawrence ND, Münkner S, Engel J, Knipper M, Magistretti J, Masetto S, Marcotti W: Elementary properties of $Ca_V1.3$ Ca^{2+} channels expressed in mouse cochlear inner hair cells. J Physiol 2010;588:187-199.

44 Dallos P, Harris D: Properties of auditory nerve responses in absence of outer hair cells. J Neurophysiol 1978;41:365-383.

45 Verpy E, Weil D, Leibovici M, Goodyear RJ, Hamard G, Houdon C, Lefevre GM, Hardelin JP, Richardson GP, Avan P, Petit C: Stereocilin-deficient mice reveal the origin of cochlear waveform distortions. Nature 2008;456:255-258.

46 Bourien J, Tang Y, Batrel C, Huet A, Lenoir M, Ladrech S, Desmadryl G, Nouvian R, Puel JL, Wang J: Contribution of auditory nerve fibers to compound action potential of the auditory nerve. J Neurophysiol 2014;112:1025-1039.

47 Durrant JD, Wang J, Ding DL, Salvi RJ: Are inner or outer hair cells the source of summating potentials recorded from the round window? J Acoust Soc Am 1998;104:370-377.

48 Patuzzi RB, Yates GK, Johnstone BM: Outer hair cell receptor current and sensorineural hearing loss. Hear Res 1989;42:47-72.

49 Belyantseva IA, Adler HJ, Curi R, Frolenkov GI, Kachar B: Expression and localization of prestin and the sugar transporter GLUT-5 during development of electromotility in cochlear outer hair cells. J Neurosci 2000;20:RC116.

50 Weber T, Zimmermann U, Winter H, Mack A, Köpschall I, Rohbock K, Zenner HP, Knipper M: Thyroid hormone is a critical determinant for the regulation of the cochlear motor protein prestin. Proc Natl Acad Sci U S A 2002;99:2901-2906.

51 Kharkovets T, Hardelin JP, Safieddine S, Schweizer M, El-Amraoui A, Petit C, Jentsch TJ: KCNQ4, a K^+ channel mutated in a form of dominant deafness, is expressed in the inner ear and the central auditory pathway. Proc Natl Acad Sci U S A 2000;97:4333-4338.
52 Beisel KW, Rocha-Sanchez SM, Morris KA, Nie L, Feng F, Kachar B, Yamoah EN, Fritzsch B: Differential expression of KCNQ4 in inner hair cells and sensory neurons is the basis of progressive high-frequency hearing loss. J Neurosci 2005;25:9285-9293.
53 Roux I, Safieddine S, Nouvian R, Grati M, Simmler MC, Bahloul A, Perfettini I, Le Gall M, Rostaing P, Hamard G, Triller A, Avan P, Moser T, Petit C: Otoferlin, defective in a human deafness form, is essential for exocytosis at the auditory ribbon synapse. Cell 2006;127:277-289.
54 Roux I, Wersinger E, McIntosh JM, Fuchs PA, Glowatzki E: Onset of cholinergic efferent synaptic function in sensory hair cells of the rat cochlea. J Neurosci 2011;31:15092-15101.
55 Zampini V, Rüttiger L, Johnson SL, Franz C, Furness DN, Waldhaus J, Xiong H, Hackney CM, Holley MC, Offenhauser N, Di Fiore PP, Knipper M, Masetto S, Marcotti W: Eps8 regulates hair bundle length and functional maturation of mammalian auditory hair cells. PLoS Biol 2011;9:e1001048, doi:10.1371/journal.pbio.1001048.
56 Katz E, Elgoyhen AB, Gomez-Casati ME, Knipper M, Vetter DE, Fuchs PA, Glowatzki E: Developmental regulation of nicotinic synapses on cochlear inner hair cells. J Neurosci 2004;24:7814-7820.
57 Marcotti W: Functional assembly of mammalian cochlear hair cells. Exp Physiol 2012;97:438-451.
58 Knipper M, Panford-Walsh R, Singer W, Rüttiger L, Zimmermann U: Specific synaptopathies diversify brain responses and hearing disorders: you lose the gain from early life. Cell Tissue Res 2015;361:77-93.
59 Kaltenbach JA, Zhang J: Intense sound-induced plasticity in the dorsal cochlear nucleus of rats: evidence for cholinergic receptor upregulation. Hearing Res 2007;226:232-243.
60 Keine C, Rubsamen R, Englitz B: Inhibition in the auditory brainstem enhances signal representation and regulates gain in complex acoustic environments. eLife 2016;5, doi:10.7554/eLife.19295.
61 Ngodup T, Goetz JA, McGuire BC, Sun W, Lauer AM, Xu-Friedman MA: Activity-dependent, homeostatic regulation of neurotransmitter release from auditory nerve fibers. Proc Nat Acad Scie USA 2015;112:6479-6484.
62 Zou J, Zhang Y, Yin S, Wu H, Pyykko I: Mitochondrial dysfunction disrupts trafficking of Kir4.1 in spiral ganglion satellite cells. J Neurosci Res 2009;87:141-149.
63 Hibino H, Horio Y, Fujita A, Inanobe A, Doi K, Gotow T, Uchiyama Y, Kubo T, Kurachi Y: Expression of an inwardly rectifying K(+) channel, Kir4.1, in satellite cells of rat cochlear ganglia. Am J Physiol 1999;277:C638-644.
64 Sonntag M, Blosa M, Schmidt S, Rubsamen R, Morawski M: Perineuronal nets in the auditory system. Hearing Res 2015;329:21-32.
65 Manor U, Kachar B: Dynamic length regulation of sensory stereocilia. Semin Cell Dev Biol 2008;19:502-510.
66 Vogl C, Butola T, Haag N, Hausrat TJ, Leitner MG, Moutschen M, Lefebvre PP, Speckmann C, Garrett L, Becker L, Fuchs H, Hrabe de Angelis M, Nietzsche S, Kessels MM, Oliver D, Kneussel M, Kilimann MW, Strenzke N: The BEACH protein LRBA is required for hair bundle maintenance in cochlear hair cells and for hearing. EMBO reports 2017.
67 Drummond MC, Barzik M, Bird JE, Zhang DS, Lechene CP, Corey DP, Cunningham LL, Friedman TB: Live-cell imaging of actin dynamics reveals mechanisms of stereocilia length regulation in the inner ear. Nat Commun 2015;6:6873.
68 Marcotti W, Corns LF, Goodyear RJ, Rzadzinska AK, Avraham KB, Steel KP, Richardson GP, Kros CJ: The acquisition of mechano-electrical transducer current adaptation in auditory hair cells requires myosin VI. J Physiol 2016;594:3667-3681.
69 Behlouli A, Bonnet C, Abdi S, Bouaita A, Lelli A, Hardelin JP, Schietroma C, Rous Y, Louha M, Cheknane A, Lebdi H, Boudjelida K, Makrelouf M, Zenati A, Petit C: EPS8, encoding an actin-binding protein of cochlear hair cell stereocilia, is a new causal gene for autosomal recessive profound deafness. Orphanet J Rare Dis 2014;9:55, doi:10.1186/1750-1172-9-55.
70 Alagramam KN, Goodyear RJ, Geng R, Furness DN, van Aken AF, Marcotti W, Kros CJ, Richardson GP: Mutations in protocadherin 15 and cadherin 23 affect tip links and mechanotransduction in mammalian sensory hair cells. PloS one 2011;6:e19183, doi:10.1371/journal.pone.0019183.

71 Barral J, Martin P: The physical basis of active mechanosensitivity by the hair-cell bundle. Curr Opin Otolaryngol Head Neck Surg 2011;19:369-375, doi:10.1097/MOO.0b013e32834a8c33.
72 Patuzzi R: Non-linear aspects of outer hair cell transduction and the temporary threshold shifts after acoustic trauma. Audiol Neurootol 2002;7:17-20.
73 Elberling C, Don M: Threshold characteristics of the human auditory brain stem response. J Acoust Soc Am 1987;81:115-121.
74 Ebrahim S, Ingham NJ, Lewis MA, Rogers MJ, Cui R, Kachar B, Pass JC, Steel KP: Alternative splice forms influence functions of whirlin in mechanosensory hair cell stereocilia. Cell Rep 2016;15:935-943.
75 Furness DN, Johnson SL, Manor U, Rüttiger L, Tocchetti A, Offenhauser N, Olt J, Goodyear RJ, Vijayakumar S, Dai Y, Hackney CM, Franz C, Di Fiore PP, Masetto S, Jones SM, Knipper M, Holley MC, Richardson GP, Kachar B, Marcotti W: Progressive hearing loss and gradual deterioration of sensory hair bundles in the ears of mice lacking the actin-binding protein Eps8L2. Proc Natl Acad Sci U S A 2013;110:13898-13903.
76 Brandt N, Kuhn S, Münkner S, Braig C, Winter H, Blin N, Vonthein R, Knipper M, Engel J: Thyroid hormone deficiency affects postnatal spiking activity and expression of Ca^{2+} and K^+ channels in rodent inner hair cells. J Neurosci 2007;27:3174-3186.
77 Sendin G, Bulankina AV, Riedel D, Moser T: Maturation of ribbon synapses in hair cells is driven by thyroid hormone. J Neurosci 2007;27:3163-3173.
78 Rüsch A, Ng L, Goodyear R, Oliver D, Lisoukov I, Vennstrom B, Richardson G, Kelley MW, Forrest D: Retardation of cochlear maturation and impaired hair cell function caused by deletion of all known thyroid hormone receptors. J Neurosci 2001;21:9792-9800.
79 Marcotti W, Johnson SL, Rüsch A, Kros CJ: Sodium and calcium currents shape action potentials in immature mouse inner hair cells. J Physiol 2003;552:743-761.
80 Heidrych P, Zimmermann U, Kuhn S, Franz C, Engel J, Duncker SV, Hirt B, Pusch CM, Ruth P, Pfister M, Marcotti W, Blin N, Knipper M: Otoferlin interacts with myosin VI: implications for maintenance of the basolateral synaptic structure of the inner hair cell. Hum Mol Genet 2009;18:2779-2790.
81 Roux I, Hosie S, Johnson SL, Bahloul A, Cayet N, Nouaille S, Kros CJ, Petit C, Safieddine S: Myosin VI is required for the proper maturation and function of inner hair cell ribbon synapses. Hum Mol Genet 2009;18:4615-4628.
82 Schaette R, McAlpine D: Tinnitus with a normal audiogram: physiological evidence for hidden hearing loss and computational model. J Neurosci 2011;31:13452-13457.
83 Heeringa AN, van Dijk P: The dissimilar time course of temporary threshold shifts and reduction of inhibition in the inferior colliculus following intense sound exposure. Hear Res 2014;312:38-47.
84 Mulders WH, Robertson D: Progressive centralization of midbrain hyperactivity after acoustic trauma. Neuroscience 2011;192:753-760.
85 Heeringa AN, Stefanescu RA, Raphael Y, Shore SE: Altered vesicular glutamate transporter distributions in the mouse cochlear nucleus following cochlear insult. Neuroscience 2016;315:114-124.
86 Claydon TW, Makary SY, Dibb KM, Boyett MR: The selectivity filter may act as the agonist-activated gate in the G protein-activated Kir3.1/Kir3.4 K+ channel. J Biol Chem 2003;278:50654-50663.
87 Otmakhova NA, Lisman JE: Contribution of Ih and GABAB to synaptically induced afterhyperpolarizations in CA1: a brake on the NMDA response. J Neurophysiol 2004;92:2027-2039.
88 Kou ZZ, Qu J, Zhang DL, Li H, Li YQ: Noise-induced hearing loss is correlated with alterations in the expression of GABAB receptors and PKC gamma in the murine cochlear nucleus complex. Frontiers Neuroanat 2013;7:25, doi:10.3389/fnana.2013.00025.
89 Lujan R, Shigemoto R, Kulik A, Juiz JM: Localization of the GABAB receptor 1a/b subunit relative to glutamatergic synapses in the dorsal cochlear nucleus of the rat. J Comp Neurol 2004;475:36-46.
90 Robel S, Sontheimer H: Glia as drivers of abnormal neuronal activity. Nature Neurosci 2016;19:28-33.
91 Igelhorst BA, Niederkinkhaus V, Karus C, Lange MD, Dietzel ID: Regulation of neuronal excitability by release of proteins from glial cells. Philos Trans R Soc Lond B Biol Sci 2015;370, doi:10.1098/rstb.2014.0194.
92 Akil O, Sun Y, Vijayakumar S, Zhang W, Ku T, Lee CK, Jones S, Grabowski GA, Lustig LR: Spiral ganglion degeneration and hearing loss as a consequence of satellite cell death in saposin B-deficient mice. J Neurosci 2015;35:3263-3275, doi:10.1523/JNEUROSCI.3920-13.2015.